
Amortized Auto-Tuning: Cost-Efficient Transfer Optimization for Hyperparameter Recommendation

Yuxin Xiao¹, Eric P. Xing^{1,3,4}, Willie Neiswanger^{2,3}

¹Carnegie Mellon University, ²Stanford University, ³Petuum, ⁴MBZUAI
yuxinxia@andrew.cmu.edu, epxing@cs.cmu.edu, neiswanger@cs.stanford.edu

Abstract

With the surge in the number of hyperparameters and training times of modern machine learning models, hyperparameter tuning is becoming increasingly expensive. Although methods have been proposed to speed up tuning via knowledge transfer, they typically require the final performance of hyperparameters and do not focus on low-fidelity information. Nevertheless, this common practice is suboptimal and can incur an unnecessary use of resources. It is more cost-efficient to instead leverage the low-fidelity tuning observations to measure inter-task similarity and transfer knowledge from existing to new tasks accordingly. However, performing multi-fidelity tuning comes with its own challenges in the transfer setting: the noise in the additional observations and the need for performance forecasting. Therefore, we conduct a thorough analysis of the multi-task multi-fidelity Bayesian optimization framework, which leads to the best instantiation—AmorTized Auto-Tuning (AT2). We further present an offline-computed 27-task Hyperparameter Recommendation (HyperRec) database to serve the community. Extensive experiments on HyperRec and other real-world databases illustrate the effectiveness of our AT2 method.¹

1 Introduction

Modern machine learning models typically come with a large number of hyperparameters and are often sensitive to their values. Consequently, researchers have paid increasing attention to automatic hyperparameter tuning [18, 22, 72], which aims to identify a set of optimal hyperparameters for a learning task without human experts. With the aid of optimization histories of past tuning sessions, some methods propose to accelerate new tuning processes via knowledge transfer. Despite their impressive results, these methods come with limitations on their cost-efficiency and flexibility, in the sense that they either make modality-specific one-time predictions [1, 6, 42, 69, 70] or rely on extra information from new tasks [11, 24, 35, 46, 52]. More importantly, they generally operate on the final performance of hyperparameters and ignore low-fidelity information [13, 55, 57, 59, 64]. As we demonstrate via a motivating example in Section 2.3, this practice incurs an unnecessary cost. It is more resource-efficient to instead utilize cheap-to-obtain low-fidelity tuning observations when carrying out inter-task hyperparameter transfer learning.

However, performing multi-fidelity tuning in the transfer setting is non-trivial. It requires carefully distilling relevant knowledge from the additional multi-fidelity information in existing tasks. It also demands accurate forecasting to extrapolate max-fidelity performance based on corresponding low-fidelity observations. To this end, we resort to the well-established approach of Bayesian optimization (BO) and conduct a thorough analysis of a multi-task multi-fidelity BO framework. In particular, we address the aforementioned challenges by considering a family of kernels and, based on an empirical evaluation, develop an AmorTized Auto-Tuning (AT2) method—the name is derived from the fact that past tuning costs will be written off in future tuning sessions.

We summarize our contributions as follows: (1) To better leverage cheap-to-obtain low-fidelity observations for measuring inter-task dependency efficiently, we conduct a thorough analysis of the

¹AT2 and HyperRec are available at <https://github.com/xiaoyuxin1002/amortized-auto-tuning>.

multi-task multi-fidelity BO framework where we empirically evaluate 64 different instantiations. (2) To motivate our analysis and as a service to the community, we present an offline-computed Hyperparameter Recommendation (HyperRec) database. It consists of 27 unique computer vision tuning tasks and 150 distinct configurations over a 16-dimensional hyperparameter space. (3) Based on the analysis, we propose the AT2 method, which uses a novel task kernel and acquisition function. It outperforms competitive baselines on HyperRec and other real-world tuning databases.

2 Background & Motivation

2.1 Preliminaries of Hyperparameter Transfer Optimization

Consider a black-box function $f : \mathcal{X} \rightarrow \mathbb{R}$ where the input space \mathcal{X} is defined as the Cartesian product of the task space \mathcal{T} , the configuration space \mathcal{C} , and the fidelity space \mathcal{E} , i.e., $\mathcal{X} = \mathcal{T} \times \mathcal{C} \times \mathcal{E}$. At each iteration, we make a (typically expensive) function evaluation and obtain a noisy observation $y = f(x) + \epsilon$ (where ϵ is drawn from some noise distribution) for an input $x \in \mathcal{X}$. Moreover, the fidelity space can only be queried in incremental order. That is, if we want to query a given $x \in \mathcal{X}$, where $x = (t, c, e)$, we must first query all $e' < e$. Consequently, it incurs a larger computational cost to acquire an observation for a higher fidelity value.

Suppose for a set of *past* tasks $\{t_i\}_{i=1}^T$, we have collected some subset of associated observations $\{y_i\}_{i=1}^N$ via querying the search space. Given a *new* task t^* , we would like to propose an optimization strategy that aims to identify $x^* = (t^*, c^*, e^*)$ using as little computation as possible with the help of knowledge transfer from offline observations. Here, c^* and e^* are where f achieves its maximum on t^* , i.e., $(c^*, e^*) = \arg \max_{c \in \mathcal{C}, e \in \mathcal{E}} f((t^*, c, e))$.

In this paper, we focus on this setup for the task of hyperparameter transfer optimization, where we treat $t \in \mathcal{T}$ as a single tuning instance, $c \in \mathcal{C}$ as a hyperparameter configuration, $e \in \mathcal{E}$ as an epoch value, and $f(x)$ as the associated validation accuracy. In particular, we are interested in two metrics for the effectiveness of an optimization strategy on a new task t^* : given query budget Q , we want to minimize the *simple regret* $R_Q = f(x^*) - \max_{q=1, \dots, Q} f(x_q)$ of queried points x_q , and maximize the *final performance* $F_Q = \max_{e \in \mathcal{E}} f((t^*, c_Q^*, e))$ of the predicted optimal configuration c_Q^* .

2.2 Limitations of Existing Work

Besides the performance metrics introduced above, we would like to further assess the cost-efficiency (**E**) and flexibility (**F**) of hyperparameter tuning methods based on the following criteria.

- E1:** (*Transferable*) The method should leverage the observations of existing tasks and perform knowledge transfer to speed up the tuning process of any new tasks.
- E2:** (*Low-fidelity*) The method should utilize low-fidelity information and not proceed with max-fidelity performance only.
- E3:** (*Cost-aware*) The method should respond to different computational costs involved in querying for observations of different tasks or fidelities.
- E4:** (*Sequential*) The method should actively adapt to any observations received while tuning new tasks and carry out feedback-driven sequential tuning.
- F1:** (*Modality-agnostic*) The method should be data modality-agnostic and broadly applicable to various data types.
- F2:** (*Self-contained*) The method should be able to operate on any new tasks without relying on auxiliary information such as extracted metadata or pre-computed representations.
- F3:** (*Cold-start friendly*) The method should be able to work well under cold start situations and not require any observations on new tasks in order to execute.

To this end, we summarize our evaluation results on existing hyperparameter recommendation literature in Table 1 and give more details in Appendix A. In general, widely-adopted Bayesian optimization (BO) methods [43] define a surrogate model (e.g., Gaussian process [28, 54], neural networks [55], random forests [21]) on the target black-box function and deploy an acquisition function (e.g., GP-UCB [2, 58] and GP-EI [25]) to determine future query points. However, vanilla BO methods focus on single-task tuning and require preliminary observations for proper initialization.

One line of extension is multi-fidelity BO methods [20, 26, 32], which apply cheap approximations to the target function. Some bandit-based [9, 38, 39] and learning curve modeling [8, 60] approaches also examine the multi-fidelity information for early stopping. Hence, they do a better job at leveraging low-fidelity information for single-task tuning, which leads to more effective resource allocation.

Category	Method	Cost-Efficiency				Flexibility		
		E1	E2	E3	E4	F1	F2	F3
Vanilla BO	DNGO [55]				✓	✓	✓	
Multi-fidelity BO	Fabolas [32]		✓	✓	✓	✓	✓	
Bandit-based approach	Hyperband [38]		✓	✓	✓	✓	✓	✓
	ABLR-HB [61]	✓	✓	✓	✓	✓	✓	✓
Multi-task BO	MTBO [59]	✓		✓	✓	✓	✓	✓
	ABLR [46]	✓			✓	✓	✓	
Recommendation method	OBOE [70]	✓						✓
Domain-specific method	HyperSTAR [42]	✓						✓
Multi-task multi-fidelity BO	AT2 [Ours]	✓	✓	✓	✓	✓	✓	✓

Table 1: Evaluation of hyperparameter tuning methods based on cost-efficiency (E) and flexibility (F). We detail the criteria in Section 2.2 and present the full table with additional methods [54, 21, 20, 26, 60, 8, 9, 39, 57, 52, 11, 64, 37, 24, 35, 30, 12, 48, 47, 3, 13, 69, 1, 6, 63] in Appendix A.

In another direction, multi-task BO methods aim to transfer knowledge between multiple optimization problems via methods such as multi-output GPs [11, 52, 59], Bayesian deep learning [57, 64], and Bayesian linear regression [46]. However, they mostly operate on the final (max-fidelity) performance and treat all queries as having equal cost. Even when equipped with the optimization histories of previous tasks, these methods often spend some budget on obtaining initial max-fidelity observations on new tasks so as to measure inter-task similarity before carrying out knowledge transfer. As we will show in the motivating example below, this procedure is unnecessary and, often, unexpectedly costly.

Towards a similar goal, some approaches view hyperparameter transfer learning from a warm-start [12, 30, 47, 48] or recommendation [3, 13, 69, 70] perspective and typically rely on pre-computed task-dependent metadata or representations. A few prediction-only methods [1, 6, 42, 63] have been proposed for specific domains but satisfy neither the sequential tuning nor modality-agnostic criteria.

On account of the analysis above, we draw merits from both multi-task and multi-fidelity BO methods and present an AmorTized Auto-Tuning (AT2) method, which fulfills each of the cost-efficiency and flexibility criteria. In particular, AT2 performs sequential, modality-free tuning of validation accuracy and transfers knowledge from existing to new tasks effectively, even under cold start scenarios, based on cheap-to-obtain low-fidelity observations (instead of auxiliary or full-fidelity information). Nevertheless, it is a non-trivial task to consider the multi-fidelity information in the transfer setting. For instance, the additional structure given by the multi-fidelity observations from previous tasks demands careful attention. Additionally, in this setting we must forecast the max-fidelity performance of hyperparameters based on their corresponding low-fidelity observations.

2.3 Motivating Example

To illustrate the challenges involved in multi-task multi-fidelity tuning, we implement a motivating example where AT2 is compared against two multi-task baselines under the cold start situation: ABLR [46], which ignores multi-fidelity information, and ABLR-HB [61], which processes multi-fidelity information via the Hyperband [38] regime. Here, we utilize a real-world hyperparameter tuning database, HyperRec (which will be introduced in detail in Section 3.1), and report the results averaged over five train-test task pairs based on the two metrics (R_Q , F_Q) discussed in Section 2.1. For F_Q , we use the *final performance ranking* of the configuration with the highest predicted mean instead of the raw score for a clearer presentation. All three methods are trained with their respective default settings and given an iteration budget four times the max fidelity (i.e., $Q = 4 \times E_{\max} = 300$).

As shown in Figure 1, since ABLR uses max-fidelity observations from the test task, its final performance ranking suffers initially and improves only after making several max-fidelity queries. Meanwhile, when ABLR is still waiting for its first max-fidelity feedback, AT2 and ABLR-HB are able to update their predictions immediately after receiving low-fidelity feedback and quickly recognize promising hyperparameter configurations. This phenomenon renders the cost of max-fidelity initialization in ABLR unnecessary and illustrates the advantage of low-fidelity tuning.

On the other hand, although Hyperband is ideal for the parallel tuning setting when substantial computational resources are accessible, it begins by selecting a large batch of configurations and thus uses excessive computation in the low-fidelity region given the same iteration budget (in terms of total computation, disregarding parallelism). As a result, in our sequential setting, ABLR-HB only

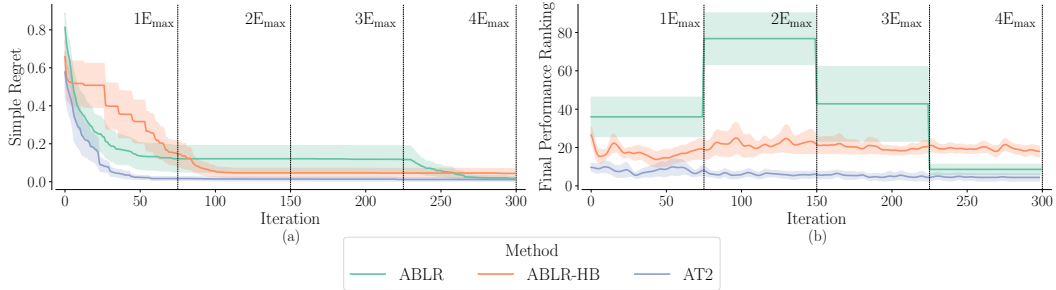


Figure 1: An example illustrating the advantages of leveraging low-fidelity observations for cost-efficient hyperparameter transfer optimization, shown on the HyperRec database (Section 3.1). Each method is allowed an iteration budget four times the max-fidelity (E_{\max}). The results are averaged across five train-test task pairs. Lower is better. The shaded regions represent one standard error of each method. Our proposed AT2 method conducts knowledge transfer based on cheap-to-get low-fidelity information and consistently outperforms the other baselines in both metrics.

achieves a lower simple regret than ABLR at around the 80th iteration. Moreover, ABLR-HB’s predicted final performance ranking declines after the 50th iteration. Since ABLR-HB treats the fidelity as a contextual variable, when more multi-fidelity observations become available on the test task, the extrapolation performance begins to suffer, as it becomes difficult to identify an informative subset of training observations and forecast full-fidelity performance. Eventually, ABLR outperforms ABLR-HB in both metrics after initializing on enough full-fidelity observations.

Unlike ABLR-HB, which leaves the task of multi-fidelity tuning to Hyperband, our proposed AT2 method sequentially selects queries for increased cost-efficiency. It quantifies inter-task dependencies based on low-fidelity information and converges to a high-ranking configuration thanks to careful forecasting of validation accuracies. In addition, AT2 also balances exploration and exploitation well and achieves a lower simple regret than ABLR from the beginning. To this end, we focus on developing a multi-task multi-fidelity BO framework and discuss AT2 in detail, in the next section.

3 Methods

3.1 Hyperparameter Recommendation (HyperRec) Database

We first illustrate the problem setting in Section 2.1 with an offline-computed Hyperparameter Recommendation database—HyperRec. HyperRec consists of 27 unique image classification tuning tasks and 150 distinct configurations composed of 16 nested hyperparameters. Each task is evaluated by each configuration for 75 epochs and repeated with two different seeds. We record the validation loss and top one, five, and ten accuracies in HyperRec. More details can be found in Appendix B.

To the best of our knowledge, this is the first hyperparameter recommendation database specifically targeting computer vision tasks. By releasing HyperRec, we seek to serve both the hyperparameter tuning and computer vision communities with a database for testing and comparing the performance of existing and future hyperparameter tuning or image classification algorithms.

3.2 Multi-Task Multi-Fidelity Bayesian Optimization Framework

In what follows, we will describe the overall multi-task multi-fidelity BO framework and then give an extensive study of different implementations. The BO paradigm is characterized by the use of a probabilistic surrogate model of the expensive black-box target $f(x)$. In this paper, we stick to the popular choice of Gaussian process (GP) for the surrogate model due to its good uncertainty quantification and leave the investigation of other options (e.g., random forest [21]) to future works. To enhance the model scalability, we adopt the stochastic variational GP regression framework [19].

A GP over the input space \mathcal{X} is a random process from \mathcal{X} to \mathbb{R} , represented by a mean function $\mu : \mathcal{X} \rightarrow \mathbb{R}$ and a kernel (i.e., covariance function) $\kappa : \mathcal{X}^2 \rightarrow \mathbb{R}_+$. If $f \sim \mathcal{GP}(\mu, \kappa)$, then we have $f(x) \sim \mathcal{N}(\mu(x), \kappa(x, x))$ for all $x \in \mathcal{X}$. Consider N offline observations $D_N = \{(x_i, y_i)\}_{i=1}^N$ from T tasks where $y_i = f(x_i) + \epsilon_i \in \mathbb{R}$ and $\epsilon_i \sim \mathcal{N}(0, \eta^2)$. We stack D_N to form $\mathbf{X} \in \mathcal{X}^N$ and $\mathbf{Y} \in \mathbb{R}^N$. When using variational inference, we also learn M inducing inputs $\mathbf{Z} \in \mathcal{X}^M$ where $M \ll N$ and the corresponding inducing variables $\mathbf{u} = f(\mathbf{Z})$. Here, we let the prior distribution $p(\mathbf{u}) = \mathcal{N}(\mathbf{0}, \mathbf{I})$ and

the variational distribution $q(\mathbf{u}) = \mathcal{N}(\mathbf{m}, \mathbf{S})$. We optimize the GP hyperparameters θ and variational parameters φ by maximizing the variational evidence lower bound (ELBO),

$$\theta^*, \varphi^* = \operatorname{argmax}_{\theta, \varphi} \text{ELBO} = \operatorname{argmax}_{\theta, \varphi} \sum_{i=1}^N \mathbb{E}_{q_{\theta, \varphi}(f(x_i))} [\log p_{\theta}(y_i | f(x_i))] - \text{KL}[q_{\varphi}(\mathbf{u}) || p(\mathbf{u})], \quad (1)$$

where $q_{\theta, \varphi}(f(x_i))$ is the marginal of $p_{\theta}(f(x_i) | \mathbf{u})q_{\varphi}(\mathbf{u})$. The predictive distribution for query x is

$$p_{\theta}(f(x) | D_N) \approx \int p_{\theta}(f(x) | \mathbf{u})q_{\varphi}(\mathbf{u}) d\mathbf{u} = \mathcal{N}(\mathbf{A}\mathbf{m}, \kappa(x, x) + \mathbf{A}(\mathbf{S} - \mathbf{K})\mathbf{A}^{\top}), \quad (2)$$

where $\mathbf{A} = \mathbf{k}\mathbf{K}^{-1}$, $\mathbf{k} \in \mathbb{R}^{1 \times M}$ with $\mathbf{k}_i = \kappa(x, z_i)$, and $\mathbf{K} \in \mathbb{R}^{M \times M}$ with $\mathbf{K}_{i,j} = \kappa(z_i, z_j)$.

After incorporating the information from previous tasks, we can construct an acquisition function $\phi : \mathcal{X} \rightarrow \mathbb{R}$ for the new tuning task t^* . The next point to query $x_q = (t^*, c_q, e_q)$ at iteration q is determined by maximizing the acquisition function, i.e., $(c_q, e_q) = \operatorname{argmax}_{c \in \mathcal{C}, e \in \mathcal{E}} \phi((t^*, c, e))$ (described in detail in Section 3.4). Then we update the model parameters according to Equation 1 after collecting an observation y_q by querying for $f(x_q) = f((t^*, c_q, e_q))$. This iterative process continues until we spend the query budget Q .

Next, we provide a thorough analysis of this general multi-task multi-fidelity BO framework, where we focus on a comparison of options for the key component—the kernel κ in Section 3.3 and conclude with the best instantiation—AmorTized Auto-Tuning (AT2) algorithm in Section 3.4.

3.3 Kernel Analysis

Since the input space \mathcal{X} is the product of three spaces, we can use a kernel with the structure

$$\kappa(x, x') = \kappa((t, c, e), (t', c', e')) = \kappa_{\mathcal{T}}(t, t') \otimes \kappa_{\mathcal{C}}(c, c') \otimes \kappa_{\mathcal{E}}(e, e'), \quad (3)$$

where \otimes denotes the Kronecker product. $\kappa_{\mathcal{T}} : \mathcal{T} \rightarrow \mathbb{R}_+$, $\kappa_{\mathcal{C}} : \mathcal{C} \rightarrow \mathbb{R}_+$, and $\kappa_{\mathcal{E}} : \mathcal{E} \rightarrow \mathbb{R}_+$ are the task, configuration, and fidelity kernels, respectively. Below we will discuss kernels that are suitable for each of the three spaces and then carry out an empirical evaluation to find the best combination.

3.3.1 Task Kernel

Based on the example in Section 2.3, we are motivated to take advantage of low-fidelity function queries to define inter-task similarity. One key observation we derived from HyperRec is that if two tasks have similar low-fidelity behaviors, they often share high-scoring configurations. For instance, ACTION40 [71] and CALTECH256 [16] are two tasks in HyperRec. As shown in Figure 2 (a), they exhibit similar low-fidelity behavior, and their top five best-performing configurations largely overlap.

Moreover, we can see that this observation is ubiquitous among all task pairs. We select two groups of pairs according to the L2 distance of their optimization landscapes (i.e., between their zero-meaned validation accuracies). As shown in Figure 2 (b), task pairs similar in L2 distance share larger portions of high-performing configurations. We, therefore, propose the `OptiLand` task kernel, which infers the similarity between a new tuning task and past tasks by comparing their low-fidelity performance, in order to perform efficient optimization via knowledge transfer.

Consider a task pair (t_1, t_2) and their respective queries $X_1 = \{(t_1, c_{1,i}, e_{1,i})\}_{i=1}^{N_1}$ and $X_2 = \{(t_2, c_{2,i}, e_{2,i})\}_{i=1}^{N_2}$. Among these queries, we focus on their overlapping subset when measuring inter-task dependency, which provides robustness against noisy multi-fidelity observations of existing tasks, as reflected in the motivating example in Section 2.3. We define a matching function to return the set of configuration-fidelity tuples for which we have queried for observations on both tasks: $M(t_1, t_2) = \{(c, e) | (t_1, c, e) \in X_1, (t_2, c, e) \in X_2\}$. The corresponding observation vectors are $\mathbf{Y}_{1|(t_1, t_2)}, \mathbf{Y}_{2|(t_1, t_2)} \in \mathbb{R}^{|M(t_1, t_2)|}$, respectively. Entries in $\mathbf{Y}_{1|(t_1, t_2)}$ and $\mathbf{Y}_{2|(t_1, t_2)}$ are min-max normalized to $[0, 1]$, shifted to have zero mean, and ordered by a common permutation of $M(t_1, t_2)$.

Hence, the distance function between the optimization landscapes of t_1 and t_2 becomes $D(t_1, t_2) = \frac{\|\mathbf{Y}_{1|(t_1, t_2)} - \mathbf{Y}_{2|(t_1, t_2)}\|_2^2}{|M(t_1, t_2)|}$. Since the observation vectors are normalized, we have $D(t_1, t_2) \in [0, 1]$.

When the number of matched observations $|M(t_1, t_2)| \leq 1$ (e.g., during initialization), we simply use a distance of $\frac{1}{2}$. Note that both observation vectors are transformed to have zero mean, since we are interested in whether the optimization landscapes of two tasks have similar shapes. In this way, two tasks will have zero distance if one’s landscape is equal to another’s shifted or scaled.

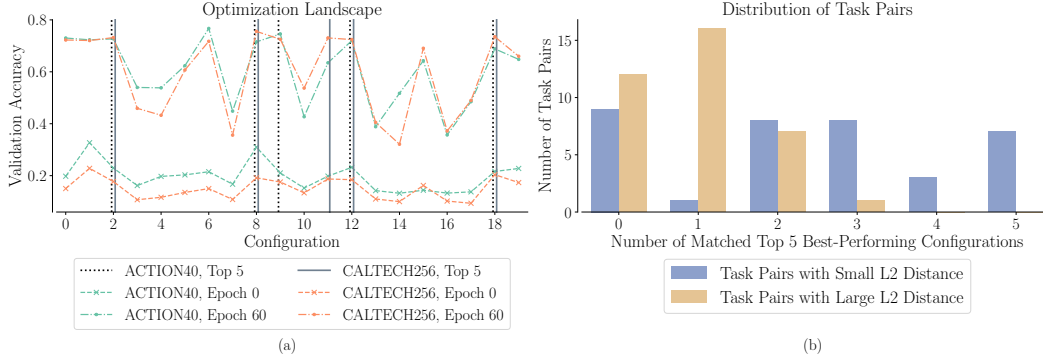


Figure 2: **(a)** Optimization landscapes of two tasks. ACTION40 and CALTECH256 have similar optimization landscapes and share a large portion of the top five best-performing configurations. **(b)** Relationship between inter-task L2 distance and the number of matched high-performing configurations. The figure shows the distributions of the top 10% of task pairs whose zero-meaned optimization landscapes are closest or farthest in terms of L2 distance. Task pairs with smaller L2 distances are more likely to share high-performing configurations.

We then define the OptiLand task kernel to assess the dependency between t_1 and t_2 as follows:

$$\kappa_{\mathcal{T}}(t_1, t_2) = \exp\left(\frac{-D(t_1, t_2)}{(\xi \cdot \gamma(t_1, t_2))^2}\right) \text{ where } \gamma(t_1, t_2) = \frac{U}{1 + (U - 1) \cdot R(t_1, t_2)}. \quad (4)$$

Here, $\xi \in \mathbb{R}_+$ is the length scale and $R(t_1, t_2) = \frac{|M(t_1, t_2)|}{|C| \times |\mathcal{E}|}$ is the ratio of matched observations. $\gamma: \mathcal{T}^2 \rightarrow \mathbb{R}_+$ is a scaling function indicating the amount of information we have about the task pair. Intuitively, no matter how many observations we have on t_1 and t_2 separately, if we have very few *matched* observations, we are less confident about how well $D(t_1, t_2)$ captures the true difference between their optimization landscapes. In this case, we would like to bias the tuning process of the new task towards existing tasks and increase the length scale to allow more knowledge transfer.

Therefore, we use a learnable parameter U to bound $\gamma \in [1, U]$. That is, when $\gamma = 1$, then the ratio of matched observations is 1, and we leave the length scale alone and let the task kernel control the amount of information transfer. Alternatively, when $\gamma = 0$, we scale up the length scale by U to increase the amount of information transfer. This design is especially useful for the cold start situation. During the early search phase of the new task, configurations queried for the new and old tasks hardly overlap. Hence, we increase the length scale via γ to allow more meaningful knowledge transfer for warm-starting the new task. This artificial upscaling is mitigated as more queries are made on the new task. Again, our claim is well supported by the good initial performance of AT2 under the cold start scenario in the motivating example (Section 2.3).

Besides the proposed OptiLand task kernel, we will compare three other possibilities for $\kappa_{\mathcal{T}}$. MTBO task kernel [59] is defined by a lookup table and optimized by learning the entries in the Cholesky decomposition of the covariance matrix. Some methods [57] also suggest learning an embedding for each task and apply a linear or second-order polynomial kernel on top of it. We name these two alternatives as DeepLinear and DeepPoly task kernels, respectively.

3.3.2 Configuration Kernel

The configuration kernel needs to deal with different hyperparameter types (i.e., numerical or categorical) and partially overlapping hyperparameter configurations. Therefore, Tree configuration kernel [41] advocates treating the configuration space as tree-structured and composites individual hyperparameter kernels in a sum-product way. For our experiments, we use an RBF or index kernel as the individual kernel for numerical or categorical hyperparameters, respectively. Alternatively, Flat configuration kernel discards the tree structure and multiplies all the individual kernels together. Some prior work [46, 57] recommends encoding the configuration space via deep learning. Hence, we construct a two-layer fully-connected neural network with *tanh* activation function and learn an embedding input for each categorical hyperparameter. Then DeepLinear or DeepPoly configuration kernels leverage a linear or second-order polynomial kernel based on network outputs, respectively.

Rank	Figure	Task Kernel	Configuration Kernel	Fidelity Kernel	ELBO
1	Figure 3 (a)	OptiLand	DeepPoly	AccCurve	1.4951
49	Figure 3 (b)	DeepPoly	DeepPoly	Matern	0.3053
64	Figure 3 (c)	MTBO	Tree	Fabolas	0.1342

Table 2: Quantitative performance of different kernel compositions. The combination of our proposed OptiLand task kernel, DeepPoly configuration kernel, and AccCurve fidelity kernel gives the highest ELBO score among the 64 candidates. Full results in Appendix C.

3.3.3 Fidelity Kernel

The fidelity kernel aims to capture how the validation accuracy changes over epochs. As inspired by [60], we define AccCurve fidelity kernel as a weighted integration over infinite basis functions: $\kappa_{\mathcal{E}}(e, e') = \int_0^{\infty} (1 - \exp\{-\lambda e\})(1 - \exp\{-\lambda e'\}) d\psi(\lambda)$. When the mixing measure ψ takes the form of a gamma distribution with parameters $\alpha, \beta > 0$, the equation can be simplified into $\kappa_{\mathcal{E}}(e, e') = 1 + (\frac{\beta}{e+e'+\beta})^{\alpha} - (\frac{\beta}{e+\beta})^{\alpha} - (\frac{\beta}{e'+\beta})^{\alpha}$. Since the basis function approximates the shape of learning curves, this kernel extrapolates the high-fidelity performance well based on low-fidelity observations. Another popular kernel for modeling multi-fidelity information is Fabolas fidelity kernel [32], where the authors assume a monotonic behavior of function evaluations with fidelity e . We also consider two simple choices for $\kappa_{\mathcal{E}}$ —RBF and Matern fidelity kernels.

3.3.4 Empirical Evaluation

In the previous sections, we discussed four options for each of the three component kernels, which gives rise to 64 combinations. Here, we identify the best-performing instantiation based on an empirical evaluation. More specifically, we randomly sample four tasks from the HyperRec database, which consists of 30,000 observations. We further sample 1,000 observations from them to form the test set and use the rest as the train set. All of the kernel combinations are trained with the same setting based on the multi-task multi-fidelity BO framework introduced in Section 3.2. Since we are concerned with how well different kernel combinations can explain the data, we report the ELBO on the test set as the quantitative metric in Table 2 (full results in Appendix C).

In general, although the other three task kernels show competitive results, the OptiLand task kernel has the best performance with different configuration and fidelity kernels. We attribute the success to its careful measurement of inter-task similarities based on matched queries. For the configuration kernel, the neural network-based kernels (i.e., DeepLinear and DeepPoly) perform better than the other two options. Finally, AccCurve fidelity kernel better models the shape of learning curves than the other three alternatives. Among the 64 candidates, the combination of OptiLand task kernel, DeepPoly configuration kernel, and AccCurve fidelity kernel achieves the highest ELBO value. Therefore, we will leverage this composition for our AT2 method in the next section.

We also provide a qualitative analysis of the kernel performance in Figure 3 (full results in Appendix C). In particular, we divide the 1,000 observations in the test set into 500 pairs and compare their *true distance*, defined by the absolute difference (which is bounded by $[0, 1]$) with the *predicted distance*, defined as $(1 - \frac{\kappa(x, x')}{\sqrt{\kappa(x, x)\kappa(x', x')}})/2 \in [0, 1]$ (given by the covariance kernel). As shown in Figure 3 (b) and (c), an ineffective kernel combination either give random or equal predicted distance regardless of the true distance. In contrast, the predicted distance by the best-performing kernel combination is more aligned with the true distance, which helps justify its quantitative result.

3.4 Amortized Auto-Tuning (AT2) Method

Besides the kernel analysis, we propose Max-Trial-GP-UCB, a specially designed acquisition function. Similar to GP-UCB [2, 58], it defines an upper confidence bound $\phi(x) = \mu(x) + \eta \cdot \sigma(x)$ on $f(x)$ for a given x . Here, $\mu(x)$ and $\sigma(x)$ are the predictive mean and standard deviation, respectively, of the posterior distribution in Equation 2. η is a hyperparameter controlling the trade-off between exploitation and exploration. Since our ultimate goal is to identify the configuration with the highest final performance on the tuning task t^* , we choose the next configuration to query as $c_q = \arg \max_{c \in \mathcal{C}} \max_{e \in \mathcal{E}} \phi((t^*, c, e))$. Suppose that for t^* and c , the maximum queried fidelity so far is $e_{\max|c}$, then we formulate the succeeding query as $x = (t^*, c, e_{\max|c} + 1)$. Unlike other multi-fidelity UCB-based acquisition functions [27], Max-Trial-GP-UCB may consider ϕ at a distinct

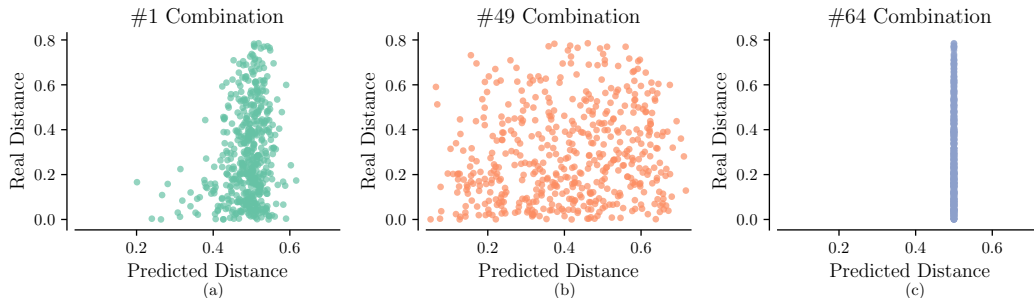


Figure 3: Qualitative performance of different kernel compositions. The highest-ranked kernel combination gives predicted distance that is relatively proportional to the real distance between query observations. Full results in Appendix C.

fidelity for each configuration. Meanwhile, it queries the fidelity space incrementally and factors in different computational costs due to the constraint in our problem setup in Section 2.1.

All together, we present the AmorTized Auto-Tuning (AT2) method as an instantiation of the multi-task multi-fidelity BO framework, consisting of OptiLand task kernel, DeepPoly configuration kernel, AccCurve fidelity kernel, and Max-Trial-GP-UCB acquisition function. AT2 measures inter-task similarity based on low-fidelity observations and enjoys the power of the best-performing kernel ensemble to transfer knowledge to new online tuning tasks in a flexible and cost-effective manner.

4 Experiments

Datasets. Besides our offline-computed database HyperRec, we consider another similar database LCBench [74] in our experiments. We sample 100 configurations from each database to construct the configuration space \mathcal{C} . Since training epochs are treated as fidelity values in our setting, we have $|\mathcal{E}| = 75$ in HyperRec and $|\mathcal{E}| = 52$ in LCBench. We further normalize the numerical hyperparameters based on their respective sampling distributions and take y to be the *top five validation accuracy* in HyperRec and the *validation balanced accuracy* in LCBench. To assess the generalizability of model performance, we randomly sample five train-test task pairs from each database where one pair consists of four training tasks and one testing task.

Baselines. We compare our AT2 method against a wide spectrum of hyperparameter transfer learning baselines: ABLR [46] applies Bayesian linear regression for each task with a shared representation space; ABLR-HB [61] further utilizes Hyperband [38] for multi-fidelity tuning; Box-BO [47] constrains the search space of BO based on the best configurations of train tasks; Box-BOHB supplies BOHB [9] with a constrained search space to allow for inter-task knowledge transfer; BOHAMIANN [57] combines neural networks with stochastic gradient Hamiltonian Monte Carlo for better scalability; PMF [13] leverages probabilistic matrix factorization for hyperparameter recommendation; RGPE [11] ensembles single-task GPs as a ranking-weighted mixture. Moreover, Box-BO uses the same configuration and fidelity kernels as AT2 for the BO process. Box-BO and Box-BOHB define the candidate pool based on the top three best-performing training configurations.

Implementation details. We implement the proposed AT2 method using the GPyTorch package [14]. More specifically, AT2 is initialized with 1,000 inducing points and optimized for 200 epochs with the momentum optimizer (learning rate = 0.02, momentum factor = 0.8) and a linearly decaying scheduler. All the other baselines are trained with their respective default settings and incorporate fidelity value as a contextual variable. We apply our novel Max-Trial-GP-UCB acquisition function to all the methods for selecting the next point to query, and after experimenting with $\{0.25, 0.5, 1\}$, we set $\eta = 0.25$ to balance exploration and exploitation.

Quantitative evaluation. To assess the performance of baselines quantitatively, we allow a query budget Q of 100 iterations and report the results averaged over five train-test task pairs for each database based on the two metrics (R_Q, F_Q) discussed in Section 2.1. Similar to Section 2.3, we use the final performance ranking for F_Q . As shown in Figure 4, although some methods give competitive simple regrets, their predicted final performance rankings deviate. In particular, methods requiring preliminary observations for proper initialization (e.g., BOHAMIANN and PMF) generally do not work well under cold start situations. The final performance rankings delivered by ABLR and ABLR-HB worsen after more observations become available, especially in HyperRec. This suggests that multi-fidelity information requires careful treatment as it is challenging to forecast max-fidelity

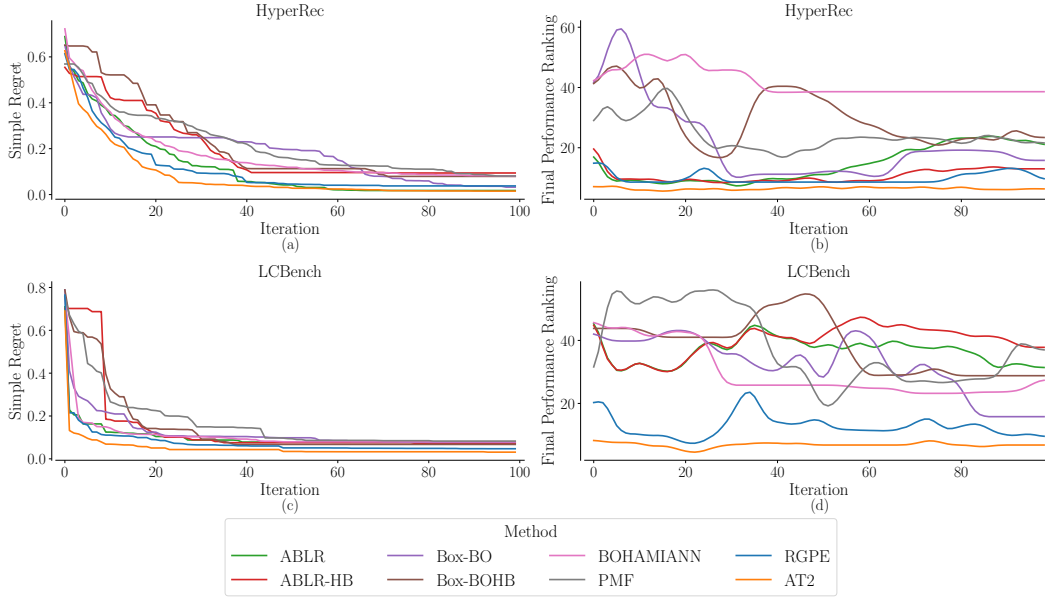


Figure 4: Performance of methods on HyperRec and LCBench. The results based on two metrics (simple regret and final performance ranking) are averaged across five train-test task pairs for each database. Lower is better. The predicted final performance rankings are smoothed with a hamming window of 10 iterations. Our proposed AT2 method consistently achieves lower values in both metrics. We omit error bars here for readability and show a version with one standard error in Appendix D.

performance. Moreover, while Box-BO shares the same configuration and fidelity kernels as AT2, it takes a much longer time for Box-BO to converge to a relatively satisfying result, which validates the significance of the task kernel in AT2. In contrast, RGPE scores well for both metrics thanks to the performance of ensemble methods. Last but not least, our proposed AT2 method outperforms other baselines by a clear margin, achieving lower simple regrets much faster and stabilizing on low final performance rankings even during the first few queries.

Qualitative analysis. To better understand how effective AT2 is in transferring knowledge and forecasting high-fidelity performance, we visualize how the predictive mean and standard deviation of the GP surrogate change over iterations. We randomly sample one train-test task pair and 10 configurations from HyperRec and compare the predicted and observed accuracies in Figure 5 (full version in Appendix D). At the start when there are no observations on the new task, AT2 exploits knowledge gained from previous tasks and produces a reasonable approximation of the true landscape albeit with high uncertainties. As more queries are made on the new task over iterations, AT2 can better extrapolate the high-fidelity performance (e.g., the zigzag shape from configuration 4 to 8) based on low-fidelity observations with a reduced standard deviation.

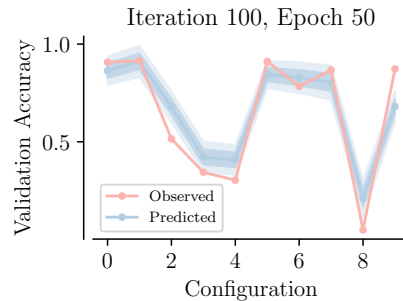


Figure 5: Extrapolation by AT2 versus true observations. The shaded region indicates one and two predictive standard deviations. Full version in Appendix D.

5 Conclusion

In this paper, to achieve cost-efficient hyperparameter transfer optimization, we focus on leveraging cheap-to-obtain low-fidelity tuning observations for measuring inter-task dependencies. Based on a thorough analysis of the multi-task multi-fidelity BO framework, we propose the AmorTized Auto-Tuning (AT2) method. We further compute a Hyperparameter Recommendation (HyperRec) database offline to serve the community. The compelling empirical performance of our AT2 method on HyperRec and other real-world databases demonstrates the method’s effectiveness. Since our analysis is currently restricted to the GP surrogate, in the future we would like to investigate how other surrogate models (e.g., random forest [21]) perform in our multi-task multi-fidelity BO framework.

References

- [1] Alessandro Achille, Michael Lam, Rahul Tewari, Avinash Ravichandran, Subhansu Maji, Charless C Fowlkes, Stefano Soatto, and Pietro Perona. Task2vec: Task embedding for meta-learning. In *Proceedings of the IEEE/CVF International Conference on Computer Vision*, pages 6430–6439, 2019.
- [2] Peter Auer. Using confidence bounds for exploitation-exploration trade-offs. *Journal of Machine Learning Research*, 3(Nov):397–422, 2002.
- [3] Rémi Bardenet, Máttyás Brendel, Balázs Kégl, and Michele Sebag. Collaborative hyperparameter tuning. In *International conference on machine learning*, pages 199–207. PMLR, 2013.
- [4] Lukas Bossard, Matthieu Guillaumin, and Luc Van Gool. Food-101 – mining discriminative components with random forests. In *European Conference on Computer Vision*, 2014.
- [5] Gong Cheng, Junwei Han, and Xiaoqiang Lu. Remote sensing image scene classification: Benchmark and state of the art. *Proceedings of the IEEE*, 105(10):1865–1883, 2017.
- [6] Yin Cui, Yang Song, Chen Sun, Andrew Howard, and Serge Belongie. Large scale fine-grained categorization and domain-specific transfer learning. In *Proceedings of the IEEE conference on computer vision and pattern recognition*, pages 4109–4118, 2018.
- [7] J. Deng, W. Dong, R. Socher, L.-J. Li, K. Li, and L. Fei-Fei. ImageNet: A Large-Scale Hierarchical Image Database. In *CVPR09*, 2009.
- [8] Tobias Domhan, Jost Tobias Springenberg, and Frank Hutter. Speeding up automatic hyperparameter optimization of deep neural networks by extrapolation of learning curves. In *Twenty-fourth international joint conference on artificial intelligence*, 2015.
- [9] Stefan Falkner, Aaron Klein, and Frank Hutter. Bohb: Robust and efficient hyperparameter optimization at scale. In *International Conference on Machine Learning*, pages 1437–1446. PMLR, 2018.
- [10] Li Fei-Fei and Pietro Perona. A bayesian hierarchical model for learning natural scene categories. In *2005 IEEE Computer Society Conference on Computer Vision and Pattern Recognition (CVPR’05)*, volume 2, pages 524–531. IEEE, 2005.
- [11] Matthias Feurer, Benjamin Letham, and Eytan Bakshy. Scalable meta-learning for bayesian optimization. *arXiv preprint arXiv:1802.02219*, 2018.
- [12] Matthias Feurer, Jost Tobias Springenberg, and Frank Hutter. Using meta-learning to initialize bayesian optimization of hyperparameters. In *MetaSel@ ECAI*, pages 3–10. Citeseer, 2014.
- [13] Nicolo Fusi, Rishit Sheth, and Melih Elibol. Probabilistic matrix factorization for automated machine learning. *Advances in neural information processing systems*, 31:3348–3357, 2018.
- [14] Jacob R Gardner, Geoff Pleiss, David Bindel, Kilian Q Weinberger, and Andrew Gordon Wilson. Gpytorch: Blackbox matrix-matrix gaussian process inference with gpu acceleration. In *Advances in Neural Information Processing Systems*, 2018.
- [15] G Geetharamani and Arun Pandian. Identification of plant leaf diseases using a nine-layer deep convolutional neural network. *Computers & Electrical Engineering*, 76:323–338, 2019.
- [16] Gregory Griffin, Alex Holub, and Pietro Perona. Caltech-256 object category dataset. 2007.
- [17] Kaiming He, Xiangyu Zhang, Shaoqing Ren, and Jian Sun. Deep residual learning for image recognition. In *Proceedings of the IEEE conference on computer vision and pattern recognition*, pages 770–778, 2016.
- [18] Xin He, Kaiyong Zhao, and Xiaowen Chu. Auttml: A survey of the state-of-the-art. *Knowledge-Based Systems*, 212:106622, 2021.
- [19] James Hensman, Alexander Matthews, and Zoubin Ghahramani. Scalable variational gaussian process classification. In *Artificial Intelligence and Statistics*, pages 351–360. PMLR, 2015.
- [20] Yi-Qi Hu, Yang Yu, Wei-Wei Tu, Qiang Yang, Yuqiang Chen, and Wenyuan Dai. Multi-fidelity automatic hyper-parameter tuning via transfer series expansion. In *Proceedings of the AAAI Conference on Artificial Intelligence*, volume 33, pages 3846–3853, 2019.
- [21] Frank Hutter, Holger H Hoos, and Kevin Leyton-Brown. Sequential model-based optimization for general algorithm configuration. In *International conference on learning and intelligent optimization*, pages 507–523. Springer, 2011.

- [22] Frank Hutter, Lars Kotthoff, and Joaquin Vanschoren. *Automated machine learning: methods, systems, challenges*. Springer Nature, 2019.
- [23] Brian Kenji Iwana, Syed Tahseen Raza Rizvi, Sheraz Ahmed, Andreas Dengel, and Seiichi Uchida. Judging a book by its cover. *arXiv preprint arXiv:1610.09204*, 2016.
- [24] Hadi S Jomaa, Lars Schmidt-Thieme, and Josif Grabocka. Hyperparameter optimization with differentiable metafeatures. *arXiv preprint arXiv:2102.03776*, 2021.
- [25] Donald R Jones, Matthias Schonlau, and William J Welch. Efficient global optimization of expensive black-box functions. *Journal of Global optimization*, 13(4):455–492, 1998.
- [26] Kirthevasan Kandasamy, Gautam Dasarathy, Junier Oliva, Jeff Schneider, and Barnabás Póczos. Gaussian process optimisation with multi-fidelity evaluations. In *Proceedings of the 30th/International Conference on Advances in Neural Information Processing Systems (NIPS’30)*, 2016.
- [27] Kirthevasan Kandasamy, Gautam Dasarathy, Jeff Schneider, and Barnabás Póczos. Multi-fidelity bayesian optimisation with continuous approximations. In *International Conference on Machine Learning*, pages 1799–1808. PMLR, 2017.
- [28] Kirthevasan Kandasamy, Karun Raju Vysyaraju, Willie Neiswanger, Biswajit Paria, Christopher R Collins, Jeff Schneider, Barnabas Poczos, and Eric P Xing. Tuning hyperparameters without grad students: Scalable and robust bayesian optimisation with dragonfly. *Journal of Machine Learning Research*, 21(81):1–27, 2020.
- [29] Aditya Khosla, Nityananda Jayadevaprakash, Bangpeng Yao, and Li Fei-Fei. Novel dataset for fine-grained image categorization. In *First Workshop on Fine-Grained Visual Categorization, IEEE Conference on Computer Vision and Pattern Recognition*, Colorado Springs, CO, June 2011.
- [30] Jungtaek Kim, Saehoon Kim, and Seungjin Choi. Learning to warm-start bayesian hyperparameter optimization. *arXiv preprint arXiv:1710.06219*, 2017.
- [31] Diederik P Kingma and Jimmy Ba. Adam: A method for stochastic optimization. *arXiv preprint arXiv:1412.6980*, 2014.
- [32] Aaron Klein, Stefan Falkner, Simon Bartels, Philipp Hennig, and Frank Hutter. Fast bayesian optimization of machine learning hyperparameters on large datasets. In *Artificial Intelligence and Statistics*, pages 528–536. PMLR, 2017.
- [33] Jonathan Krause, Michael Stark, Jia Deng, and Li Fei-Fei. 3d object representations for fine-grained categorization. In *4th International IEEE Workshop on 3D Representation and Recognition (3dRR-13)*, Sydney, Australia, 2013.
- [34] Alex Krizhevsky, Geoffrey Hinton, et al. Learning multiple layers of features from tiny images. 2009.
- [35] Ho Chung Leon Law, Peilin Zhao, Lucian Chan, Junzhou Huang, and Dino Sejdinovic. Hyperparameter learning via distributional transfer. *arXiv preprint arXiv:1810.06305*, 2018.
- [36] Svetlana Lazebnik, Cordelia Schmid, and Jean Ponce. Beyond bags of features: Spatial pyramid matching for recognizing natural scene categories. In *2006 IEEE Computer Society Conference on Computer Vision and Pattern Recognition (CVPR’06)*, volume 2, pages 2169–2178. IEEE, 2006.
- [37] Benjamin Letham and Eytan Bakshy. Bayesian optimization for policy search via online-offline experimentation. *Journal of Machine Learning Research*, 20(145):1–30, 2019.
- [38] Lisha Li, Kevin Jamieson, Giulia DeSalvo, Afshin Rostamizadeh, and Ameet Talwalkar. Hyperband: A novel bandit-based approach to hyperparameter optimization. *The Journal of Machine Learning Research*, 18(1):6765–6816, 2017.
- [39] Yang Li, Yu Shen, Jiawei Jiang, Jinyang Gao, Ce Zhang, and Bin Cui. Mfes-hb: Efficient hyperband with multi-fidelity quality measurements. *arXiv preprint arXiv:2012.03011*, 2020.
- [40] Ilya Loshchilov and Frank Hutter. Sgdr: Stochastic gradient descent with warm restarts. *arXiv preprint arXiv:1608.03983*, 2016.
- [41] Xingchen Ma and Matthew Blaschko. Additive tree-structured covariance function for conditional parameter spaces in bayesian optimization. In *International Conference on Artificial Intelligence and Statistics*, pages 1015–1025. PMLR, 2020.

- [42] Gaurav Mittal, Chang Liu, Nikolaos Karianakis, Victor Fragoso, Mei Chen, and Yun Fu. Hyperstar: Task-aware hyperparameters for deep networks. In *Proceedings of the IEEE/CVF Conference on Computer Vision and Pattern Recognition (CVPR)*, June 2020.
- [43] Jonas Mockus, Vytautas Tiesis, and Antanas Zilinskas. The application of bayesian methods for seeking the extremum. *Towards global optimization*, 2(117-129):2, 1978.
- [44] Maria-Elena Nilsback and Andrew Zisserman. Automated flower classification over a large number of classes. In *2008 Sixth Indian Conference on Computer Vision, Graphics & Image Processing*, pages 722–729. IEEE, 2008.
- [45] Omkar M Parkhi, Andrea Vedaldi, Andrew Zisserman, and CV Jawahar. Cats and dogs. In *2012 IEEE conference on computer vision and pattern recognition*, pages 3498–3505. IEEE, 2012.
- [46] Valerio Perrone, Rodolphe Jenatton, Matthias Seeger, and Cédric Archambeau. Scalable hyperparameter transfer learning. In *Proceedings of the 32nd International Conference on Neural Information Processing Systems*, pages 6846–6856, 2018.
- [47] Valerio Perrone, Huibin Shen, Matthias Seeger, Cedric Archambeau, and Rodolphe Jenatton. Learning search spaces for bayesian optimization: Another view of hyperparameter transfer learning. *arXiv preprint arXiv:1909.12552*, 2019.
- [48] Matthias Poloczek, Jialei Wang, and Peter I Frazier. Warm starting bayesian optimization. In *2016 Winter Simulation Conference (WSC)*, pages 770–781. IEEE, 2016.
- [49] Boris T Polyak. Some methods of speeding up the convergence of iteration methods. *Ussr computational mathematics and mathematical physics*, 4(5):1–17, 1964.
- [50] Ariadna Quattoni and Antonio Torralba. Recognizing indoor scenes. In *2009 IEEE Conference on Computer Vision and Pattern Recognition*, pages 413–420. IEEE, 2009.
- [51] Olga Russakovsky, Jia Deng, Hao Su, Jonathan Krause, Sanjeev Satheesh, Sean Ma, Zhiheng Huang, Andrej Karpathy, Aditya Khosla, Michael Bernstein, Alexander C. Berg, and Li Fei-Fei. ImageNet Large Scale Visual Recognition Challenge. *International Journal of Computer Vision (IJCV)*, 115(3):211–252, 2015.
- [52] David Salinas, Huibin Shen, and Valerio Perrone. A quantile-based approach for hyperparameter transfer learning. In *International Conference on Machine Learning*, pages 8438–8448. PMLR, 2020.
- [53] Leslie N Smith. Cyclical learning rates for training neural networks. In *2017 IEEE winter conference on applications of computer vision (WACV)*, pages 464–472. IEEE, 2017.
- [54] Jasper Snoek, Hugo Larochelle, and Ryan P Adams. Practical bayesian optimization of machine learning algorithms. *arXiv preprint arXiv:1206.2944*, 2012.
- [55] Jasper Snoek, Oren Rippel, Kevin Swersky, Ryan Kiros, Nadathur Satish, Narayanan Sundaram, Mostofa Patwary, Mr Prabhat, and Ryan Adams. Scalable bayesian optimization using deep neural networks. In *International conference on machine learning*, pages 2171–2180. PMLR, 2015.
- [56] Hyun Oh Song, Yu Xiang, Stefanie Jegelka, and Silvio Savarese. Deep metric learning via lifted structured feature embedding. In *IEEE Conference on Computer Vision and Pattern Recognition (CVPR)*, 2016.
- [57] Jost Tobias Springenberg, Aaron Klein, Stefan Falkner, and Frank Hutter. Bayesian optimization with robust bayesian neural networks. In *Proceedings of the 30th International Conference on Neural Information Processing Systems*, pages 4141–4149, 2016.
- [58] Niranjan Srinivas, Andreas Krause, Sham Kakade, and Matthias W Seeger. Gaussian process optimization in the bandit setting: No regret and experimental design. In *ICML*, 2010.
- [59] Kevin Swersky, Jasper Snoek, and Ryan Prescott Adams. Multi-task bayesian optimization. 2013.
- [60] Kevin Swersky, Jasper Snoek, and Ryan Prescott Adams. Freeze-thaw bayesian optimization. *arXiv preprint arXiv:1406.3896*, 2014.
- [61] Lazar Valkov, Rodolphe Jenatton, Fela Winkelmolen, and Cédric Archambeau. A simple transfer-learning extension of hyperband. In *NIPS Workshop on Meta-Learning*, 2018.
- [62] C. Wah, S. Branson, P. Welinder, P. Perona, and S. Belongie. The Caltech-UCSD Birds-200-2011 Dataset. Technical Report CNS-TR-2011-001, California Institute of Technology, 2011.

- [63] Ying Wei, Peilin Zhao, Huaxiu Yao, and Junzhou Huang. Transferable neural processes for hyperparameter optimization. *arXiv preprint arXiv:1909.03209*, 2019.
- [64] Martin Wistuba and Josif Grabocka. Few-shot bayesian optimization with deep kernel surrogates. *arXiv preprint arXiv:2101.07667*, 2021.
- [65] Xiaoping Wu, Chi Zhan, Yukun Lai, Ming-Ming Cheng, and Jufeng Yang. Ip102: A large-scale benchmark dataset for insect pest recognition. In *IEEE CVPR*, pages 8787–8796, 2019.
- [66] Yongqin Xian, Christoph H Lampert, Bernt Schiele, and Zeynep Akata. Zero-shot learning—a comprehensive evaluation of the good, the bad and the ugly. *IEEE transactions on pattern analysis and machine intelligence*, 41(9):2251–2265, 2018.
- [67] Jianxiong Xiao, Krista A Ehinger, James Hays, Antonio Torralba, and Aude Oliva. Sun database: Exploring a large collection of scene categories. *International Journal of Computer Vision*, 119(1):3–22, 2016.
- [68] Jianxiong Xiao, James Hays, Krista A Ehinger, Aude Oliva, and Antonio Torralba. Sun database: Large-scale scene recognition from abbey to zoo. In *2010 IEEE computer society conference on computer vision and pattern recognition*, pages 3485–3492. IEEE, 2010.
- [69] Chao Xue, Junchi Yan, Rong Yan, Stephen M Chu, Yonggang Hu, and Yonghua Lin. Transferable automl by model sharing over grouped datasets. In *Proceedings of the IEEE/CVF Conference on Computer Vision and Pattern Recognition*, pages 9002–9011, 2019.
- [70] Chengrun Yang, Yuji Akimoto, Dae Won Kim, and Madeleine Udell. Oboe: Collaborative filtering for automl model selection. In *Proceedings of the 25th ACM SIGKDD International Conference on Knowledge Discovery & Data Mining*, pages 1173–1183, 2019.
- [71] Bangpeng Yao, Xiaoye Jiang, Aditya Khosla, Andy Lai Lin, Leonidas Guibas, and Li Fei-Fei. Human action recognition by learning bases of action attributes and parts. In *2011 International conference on computer vision*, pages 1331–1338. IEEE, 2011.
- [72] Quanming Yao, Mengshuo Wang, Yuqiang Chen, Wenyuan Dai, Yu-Feng Li, Wei-Wei Tu, Qiang Yang, and Yang Yu. Taking human out of learning applications: A survey on automated machine learning. *arXiv preprint arXiv:1810.13306*, 2018.
- [73] Bolei Zhou, Agata Lapedriza, Aditya Khosla, Aude Oliva, and Antonio Torralba. Places: A 10 million image database for scene recognition. *IEEE Transactions on Pattern Analysis and Machine Intelligence*, 2017.
- [74] Lucas Zimmer, Marius Lindauer, and Frank Hutter. Auto-pytorch tabular: Multi-fidelity metalearning for efficient and robust autodl. *arXiv preprint arXiv:2006.13799*, 2020.

Appendix

A Cost-Efficiency and Flexibility of Existing Work

We assess the cost-efficiency (**E**) and flexibility (**F**) of hyperparameter tuning methods, based on the seven criteria detailed in Section 2.2. In the table below, we extend Table 1 (from Section 2.2) to include a full set of hyperparameter tuning methods.

Category	Method	Cost-Efficiency				Flexibility		
		E1	E2	E3	E4	F1	F2	F3
Vanilla BO	DNGO [55]				✓	✓	✓	
	GPBO [54]			✓	✓	✓	✓	
	ROAR [21]			✓	✓	✓	✓	
Multi-fidelity BO	Fabolas [32]		✓	✓	✓	✓	✓	
	TSE [20]		✓	✓	✓	✓	✓	
	MF-GP-UCB [26]		✓	✓	✓	✓	✓	
Learning curve modeling	Freeze-Thaw [60]		✓	✓	✓	✓	✓	
	LC Pred [8]		✓	✓	✓	✓	✓	
Bandit-based approach	Hyperband [38]		✓	✓	✓	✓	✓	✓
	BOHB [9]		✓	✓	✓	✓	✓	✓
	MFES-HB [39]		✓	✓	✓	✓	✓	✓
	ABLR-HB [61]	✓	✓	✓	✓	✓	✓	✓
Multi-task BO	MTBO [59]	✓		✓	✓	✓	✓	✓
	BOHAMIANN [57]	✓			✓	✓	✓	✓
	ABLR [46]	✓			✓	✓	✓	
	GCP [52]	✓			✓	✓	✓	
	RGPE [11]	✓			✓	✓	✓	
	FSBO [64]	✓			✓	✓	✓	
	Policy Search [37]	✓			✓	✓	✓	
	DMFBS [24]	✓			✓	✓		✓
distGP [35]	✓			✓			✓	
Warm-starting method	Siamese-BHO [30]	✓			✓	✓		✓
	MI-SMBO [12]	✓			✓	✓		✓
	wsKG [48]	✓			✓	✓	✓	
	Box BO [47]	✓			✓	✓	✓	
Recommendation method	SCoT [3]	✓			✓	✓	✓	
	PMF [13]	✓			✓	✓	✓	
	Data Grouping [69]	✓						✓
	OBOE [70]	✓						✓
Domain-specific method	task2vec [1]	✓						✓
	DSTL [6]	✓						✓
	HyperSTAR [42]	✓						✓
	TNP [63]	✓			✓			
Multi-task multi-fidelity BO	AT2 [Ours]	✓	✓	✓	✓	✓	✓	✓

Table 3: Evaluation of hyperparameter tuning methods based on cost-efficiency (**E**) and flexibility (**F**). **E1**: transferable; **E2**: low-fidelity; **E3**: cost-aware; **E4**: sequential; **F1**: modality-agnostic; **F2**: self-contained; **F3**: cold-start friendly. The details of these criteria are explained in Section 2.2.

B Generation of HyperRec Database

B.1 HyperRec Details

The Hyperparameter Recommendation database (HyperRec) consists of 27 unique image classification tasks and 150 distinct configurations sampled from a 16-dimensional nested hyperparameter space. The original image classification dataset of each task is split based on a common ratio: 60% for the training set, 20% for the validation set, and 20% for the testing set. We summarize the details of the tasks in Table 4 and explain the nested hyperparameter space in Appendix B.2.

For each task, we evaluate each configuration during 75 training epochs and repeat this with two randomly sampled seeds. During training, we record the batch-wise cross-entropy loss, the batch-wise top one, five, and ten accuracies, and the training time taken to loop through all the batches. During evaluation, we record the epoch-wise cross-entropy loss and the epoch-wise top one, five, and ten accuracies for the validation and testing sets separately, as well as the evaluation time taken to loop through the two sets.

Task/Dataset	Number of Images	Number of Classes
ACTION40 [71]	9,532	40
AWA2 [66]	37,322	50
BOOKCOVER30 [23]	57,000	30
CALTECH256 [16]	30,607	257
CARS196 [33]	16,185	196
CIFAR10 [34]	60,000	10
CIFAR100 [34]	60,000	100
CUB200 [62]	11,788	200
FLOWER102 [44]	8,189	102
FOOD101 [4]	101,000	101
IMAGENET64SUB1 [51]	128,112	1,000
IMAGENET64SUB2 [51]	128,112	1,000
IMAGENET64SUB3 [51]	128,112	1,000
IP102 [65]	75,222	102
ISR [50]	15,620	67
OIPETS [45]	7,349	37
PLACE365SUB1 [73]	91,987	365
PLACE365SUB2 [73]	91,987	365
PLACE365SUB3 [73]	91,987	365
PLANT39 [15]	61,486	39
RESISC45 [5]	31,500	45
SCENE15 [10, 36]	4,485	15
SDD [29, 7]	20,580	120
SOP [56]	120,053	12
SUN397SUB1 [68, 67]	9,925	397
SUN397SUB2 [68, 67]	9,925	397
SUN397SUB3 [68, 67]	9,925	397

Table 4: Details on the 27 tasks in HyperRec.

B.2 Nested Hyperparameter Space

Here, we explain the 16-dimensional nested hyperparameter space used in HyperRec. In what follows, $\mathcal{C}\{\cdot\cdot\cdot\}$ denotes the categorical distribution, $\mathcal{U}(\cdot, \cdot)$ denotes the uniform distribution, $\mathcal{U}\{\cdot, \cdot\}$ denotes the discrete uniform distribution, $\mathcal{LU}(\cdot, \cdot)$ denotes the log-uniform distribution, and CAWR stands for `CosineAnnealingWarmRestarts`.

In Table 5, we summarize information about the subset of hyperparameters in HyperRec that are independent of any categorical variables.

Hyperparameter	Tuning Distribution
Batch size	$\mathcal{U}\{32, 128\}$
Model	$\mathcal{C}\{\text{ResNet34}, \text{ResNet50}\}$
Optimizer	$\mathcal{C}\{\text{Adam}, \text{Momentum}\}$
LR Scheduler	$\mathcal{C}\{\text{StepLR}, \text{ExponentialLR}, \text{CyclicLR}, \text{CAWR}\}$

Table 5: Details on the hyperparameters that are independent of any categorical variables in HyperRec.

HyperRec involves three categorical hyperparameters: Model, Optimizer, and Learning Rate (LR) Scheduler. In particular, we consider two choices for Model (ResNet34 and ResNet50 [17]), two choices for Optimizer (Adam [31] and Momentum [49]), and four choices for LR Scheduler (StepLR, ExponentialLR, CyclicLR [53], CAWR [40]). The dependent hyperparameters of the categorical variables Optimizer and LR Scheduler in HyperRec are described in Table 6 and Table 7, respectively. Note that the categorical variable Model does not have any dependent hyperparameters in HyperRec.

Optimizer Choice	Hyperparameter	Tuning Distribution
Adam	Learning rate	$\mathcal{LU}(10^{-4}, 10^{-1})$
	Weight decay	$\mathcal{LU}(10^{-5}, 10^{-3})$
	Beta ₀	$\mathcal{LU}(0.5, 0.999)$
	Beta ₁	$\mathcal{LU}(0.8, 0.999)$
Momentum	Learning rate	$\mathcal{LU}(10^{-4}, 10^{-1})$
	Weight decay	$\mathcal{LU}(10^{-5}, 10^{-3})$
	Momentum factor	$\mathcal{LU}(10^{-3}, 1)$

Table 6: Details on the hyperparameters that are dependent on Optimizer choices in HyperRec.

LR Scheduler Choice	Hyperparameter	Tuning Distribution
StepLR	Step size	$\mathcal{U}\{2, 20\}$
	Gamma	$\mathcal{LU}(0.1, 0.5)$
ExponentialLR	Gamma	$\mathcal{LU}(0.85, 0.999)$
CyclicLR	Gamma	$\mathcal{LU}(0.1, 0.5)$
	Max learning rate	$\min(1, \text{LR} \times \mathcal{U}(1.1, 1.5))$
	Step size up	$\mathcal{U}\{1, 10\}$
CAWR	T ₀	$\mathcal{U}\{2, 20\}$
	T _{mult}	$\mathcal{U}\{1, 4\}$
	Eta _{min}	$\text{LR} \times \mathcal{U}(0.5, 0.9)$

Table 7: Details on the hyperparameters that are dependent on LR Scheduler choices in HyperRec.

C Analysis Results of Kernel Combinations

Based on the four options proposed for each of the three component kernels (task, configuration, and fidelity kernels) in Section 3.3, we empirically evaluate the resulting 64 combinations via both quantitative and qualitative measures. We discuss the evaluation results in Section 3.3.4 and present shorter versions of the following tables and figures in Table 2 and Figure 3, respectively.

Rank	Figure	Task Kernel	Configuration Kernel	Fidelity Kernel	ELBO
1	Figure 6 (a)	OptiLand	DeepPoly	AccCurve	1.4951
2	Figure 6 (b)	MTBO	DeepLinear	Matern	1.4296
3	Figure 6 (c)	OptiLand	DeepLinear	AccCurve	1.4172
4	Figure 6 (d)	OptiLand	DeepPoly	Matern	1.4127
5	Figure 6 (e)	MTBO	DeepPoly	AccCurve	1.4121
6	Figure 6 (f)	DeepPoly	DeepLinear	AccCurve	1.4017
7	Figure 6 (g)	OptiLand	DeepLinear	Matern	1.3871
8	Figure 6 (h)	DeepLinear	DeepPoly	RBF	1.3763
9	Figure 6 (i)	DeepPoly	DeepLinear	Matern	1.3700

Table 8: Quantitative performance of different kernel compositions (ranking #1 ~ #9).

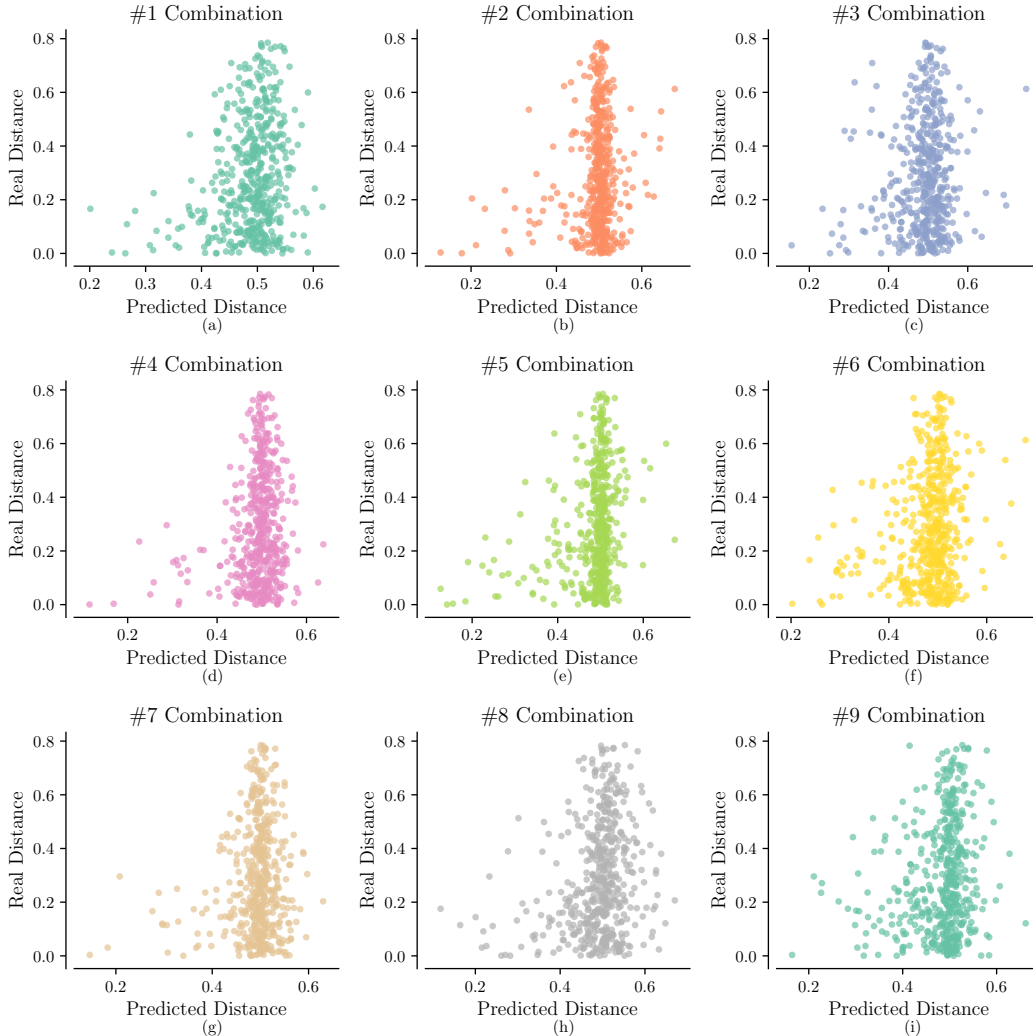


Figure 6: Qualitative performance of different kernel compositions (ranking #1 ~ #9).

Rank	Figure	Task Kernel	Configuration Kernel	Fidelity Kernel	ELBO
10	Figure 7 (a)	OptiLand	DeepLinear	RBF	1.3590
11	Figure 7 (b)	DeepLinear	DeepLinear	RBF	1.3586
12	Figure 7 (c)	DeepLinear	DeepLinear	Matern	1.3464
13	Figure 7 (d)	DeepPoly	DeepLinear	RBF	1.3460
14	Figure 7 (e)	DeepPoly	DeepPoly	RBF	1.3360
15	Figure 7 (f)	MTBO	DeepLinear	AccCurve	1.3350
16	Figure 7 (g)	DeepLinear	DeepLinear	AccCurve	1.3309
17	Figure 7 (h)	MTBO	DeepLinear	RBF	1.3170
18	Figure 7 (i)	OptiLand	Tree	AccCurve	1.3129

Table 9: Quantitative performance of different kernel compositions (ranking #10 ~ #18).

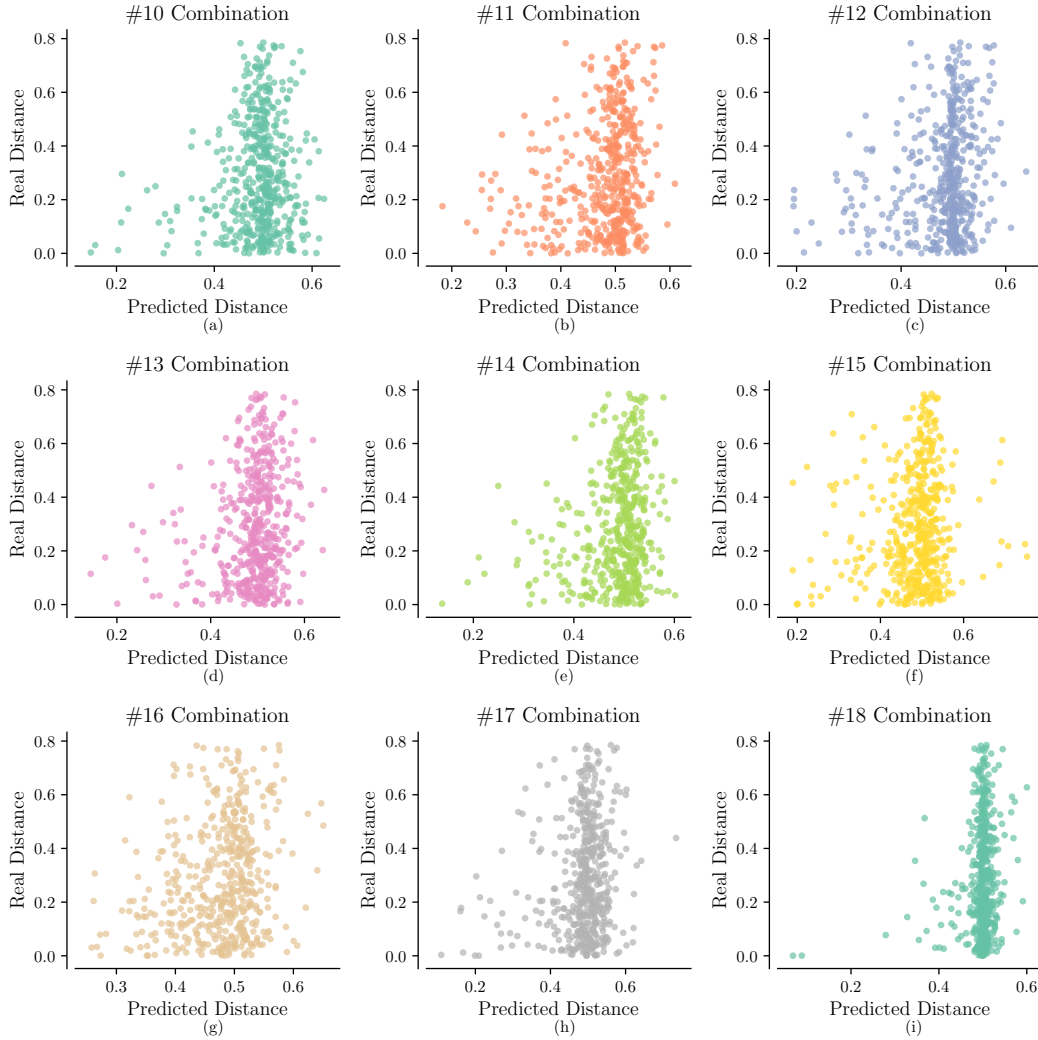


Figure 7: Qualitative performance of different kernel compositions (ranking #10 ~ #18).

Rank	Figure	Task Kernel	Configuration Kernel	Fidelity Kernel	ELBO
19	Figure 8 (a)	OptiLand	DeepPoly	RBF	1.2934
20	Figure 8 (b)	DeepPoly	DeepPoly	AccCurve	1.2925
21	Figure 8 (c)	DeepLinear	DeepPoly	AccCurve	1.2861
22	Figure 8 (d)	DeepLinear	Tree	AccCurve	1.2777
23	Figure 8 (e)	MTBO	DeepPoly	Matern	1.2763
24	Figure 8 (f)	DeepLinear	DeepPoly	Matern	1.2716
25	Figure 8 (g)	DeepPoly	Tree	AccCurve	1.2704
26	Figure 8 (h)	MTBO	DeepPoly	RBF	1.2495
27	Figure 8 (i)	OptiLand	Flat	AccCurve	1.2409

Table 10: Quantitative performance of different kernel compositions (ranking #19 ~ #27).

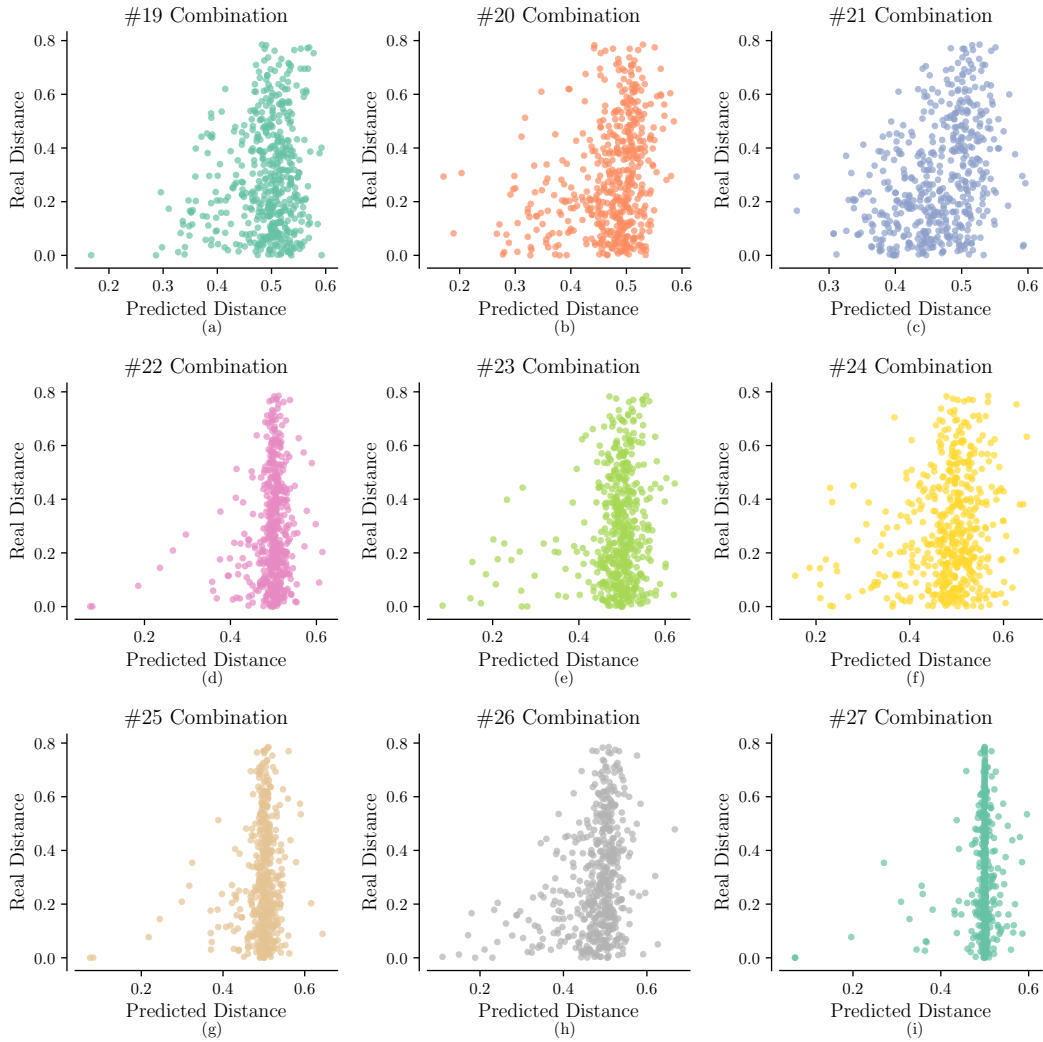


Figure 8: Qualitative performance of different kernel compositions (ranking #19 ~ #27).

Rank	Figure	Task Kernel	Configuration Kernel	Fidelity Kernel	ELBO
28	Figure 9 (a)	MTBO	Tree	AccCurve	1.2121
29	Figure 9 (b)	OptiLand	Tree	Matern	1.1843
30	Figure 9 (c)	OptiLand	Tree	RBF	1.1628
31	Figure 9 (d)	DeepPoly	Tree	Matern	1.1532
32	Figure 9 (e)	DeepPoly	Tree	RBF	1.1431
33	Figure 9 (f)	MTBO	Tree	RBF	1.0923
34	Figure 9 (g)	MTBO	Tree	Matern	1.0864
35	Figure 9 (h)	DeepLinear	Tree	Matern	1.0861
36	Figure 9 (i)	DeepLinear	Tree	RBF	1.0850

Table 11: Quantitative performance of different kernel compositions (ranking #28 ~ #36).

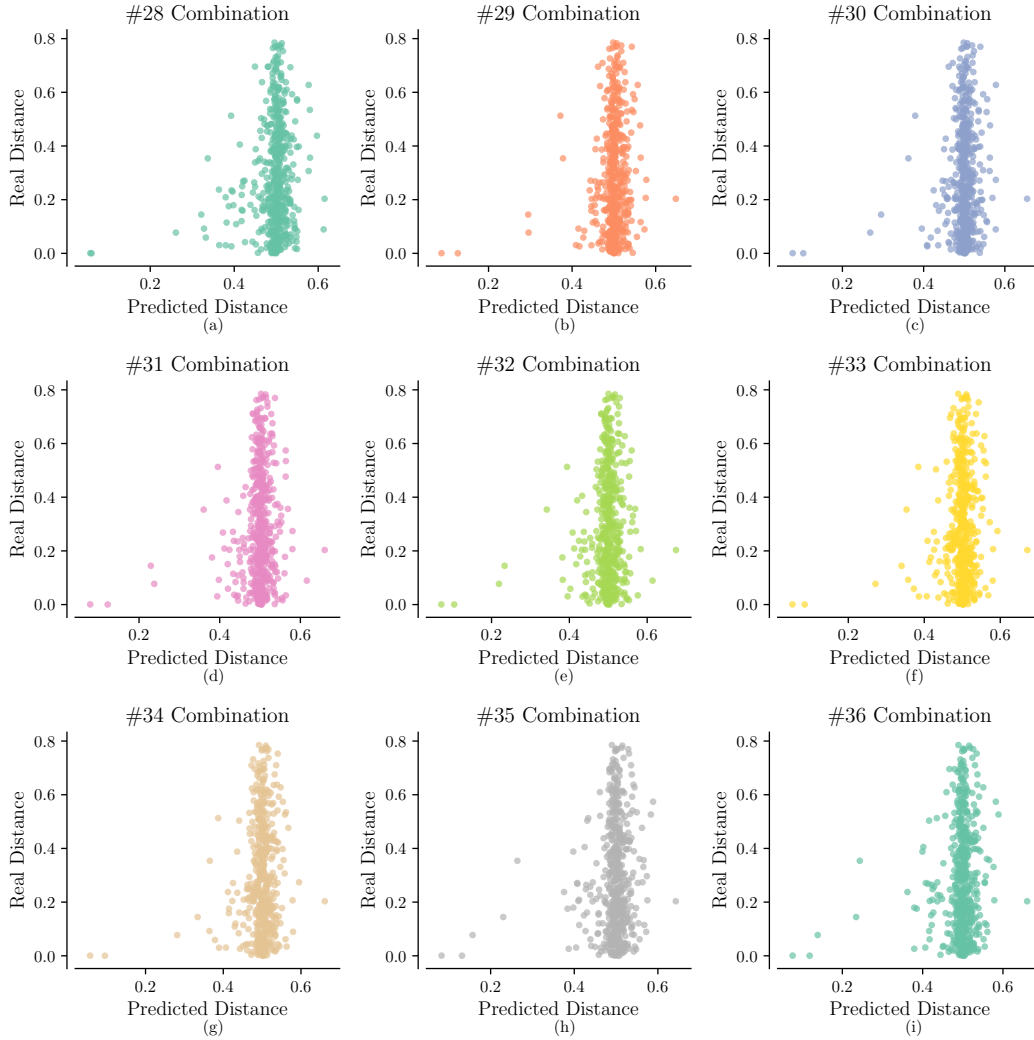


Figure 9: Qualitative performance of different kernel compositions (ranking #28 ~ #36).

Rank	Figure	Task Kernel	Configuration Kernel	Fidelity Kernel	ELBO
37	Figure 10 (a)	OptiLand	Flat	RBF	1.0633
38	Figure 10 (b)	OptiLand	Flat	Matern	1.0557
39	Figure 10 (c)	OptiLand	DeepPoly	Fabolas	1.0424
40	Figure 10 (d)	DeepPoly	Flat	AccCurve	1.0389
41	Figure 10 (e)	DeepPoly	DeepLinear	Fabolas	0.9881
42	Figure 10 (f)	DeepLinear	DeepPoly	Fabolas	0.9880
43	Figure 10 (g)	OptiLand	Tree	Fabolas	0.9224
44	Figure 10 (h)	OptiLand	Flat	Fabolas	0.9170
45	Figure 10 (i)	DeepPoly	Flat	RBF	0.9100

Table 12: Quantitative performance of different kernel compositions (ranking #37 ~ #45).

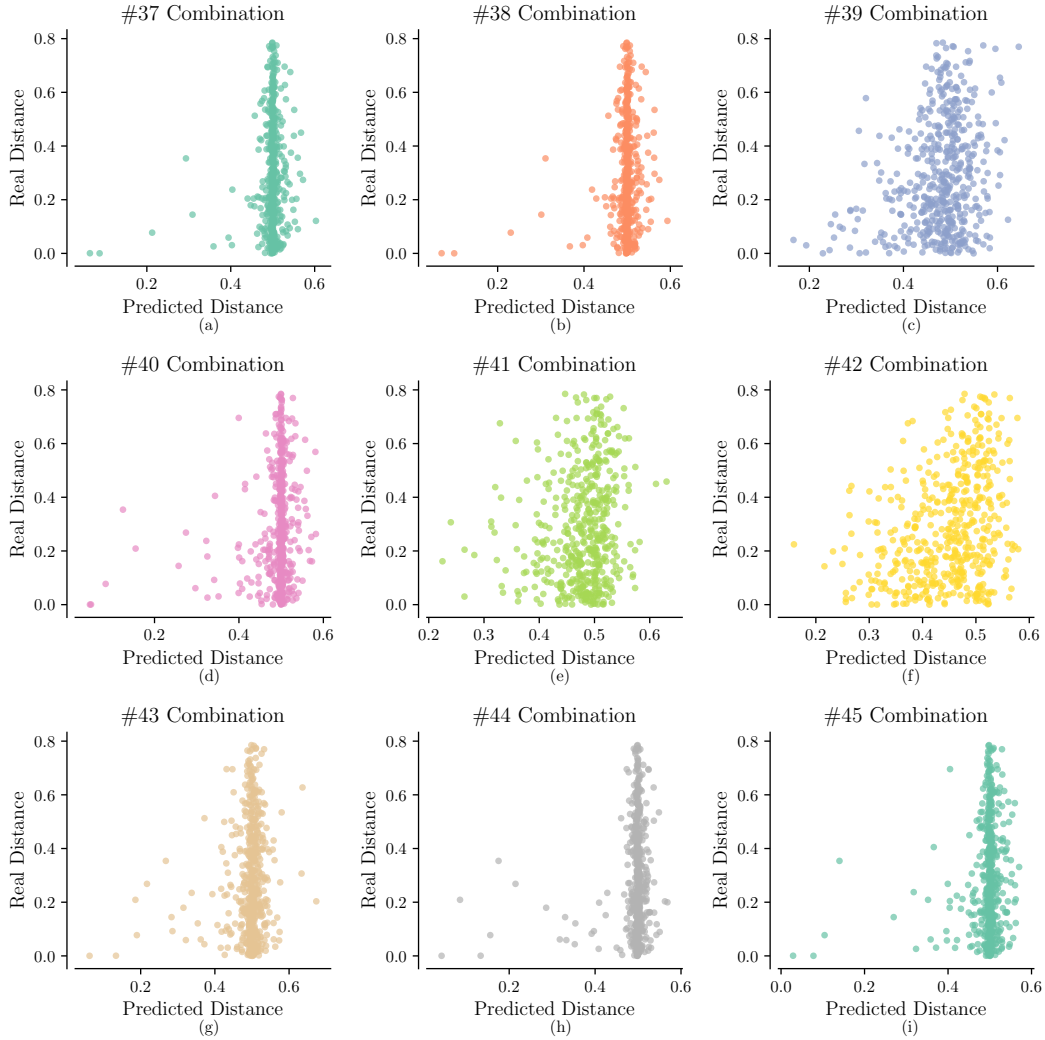


Figure 10: Qualitative performance of different kernel compositions (ranking #37 ~ #45).

Rank	Figure	Task Kernel	Configuration Kernel	Fidelity Kernel	ELBO
46	Figure 11 (a)	DeepPoly	Flat	Matern	0.8844
47	Figure 11 (b)	DeepLinear	Flat	AccCurve	0.4301
48	Figure 11 (c)	DeepLinear	Flat	RBF	0.3416
49	Figure 11 (d)	DeepPoly	DeepPoly	Matern	0.3053
50	Figure 11 (e)	MTBO	Flat	AccCurve	0.2985
51	Figure 11 (f)	DeepLinear	Flat	Matern	0.2822
52	Figure 11 (g)	MTBO	Flat	RBF	0.1433
53	Figure 11 (h)	MTBO	Flat	Matern	0.1406
54	Figure 11 (i)	DeepPoly	DeepPoly	Fabolas	0.1350

Table 13: Quantitative performance of different kernel compositions (ranking #46 ~ #54).

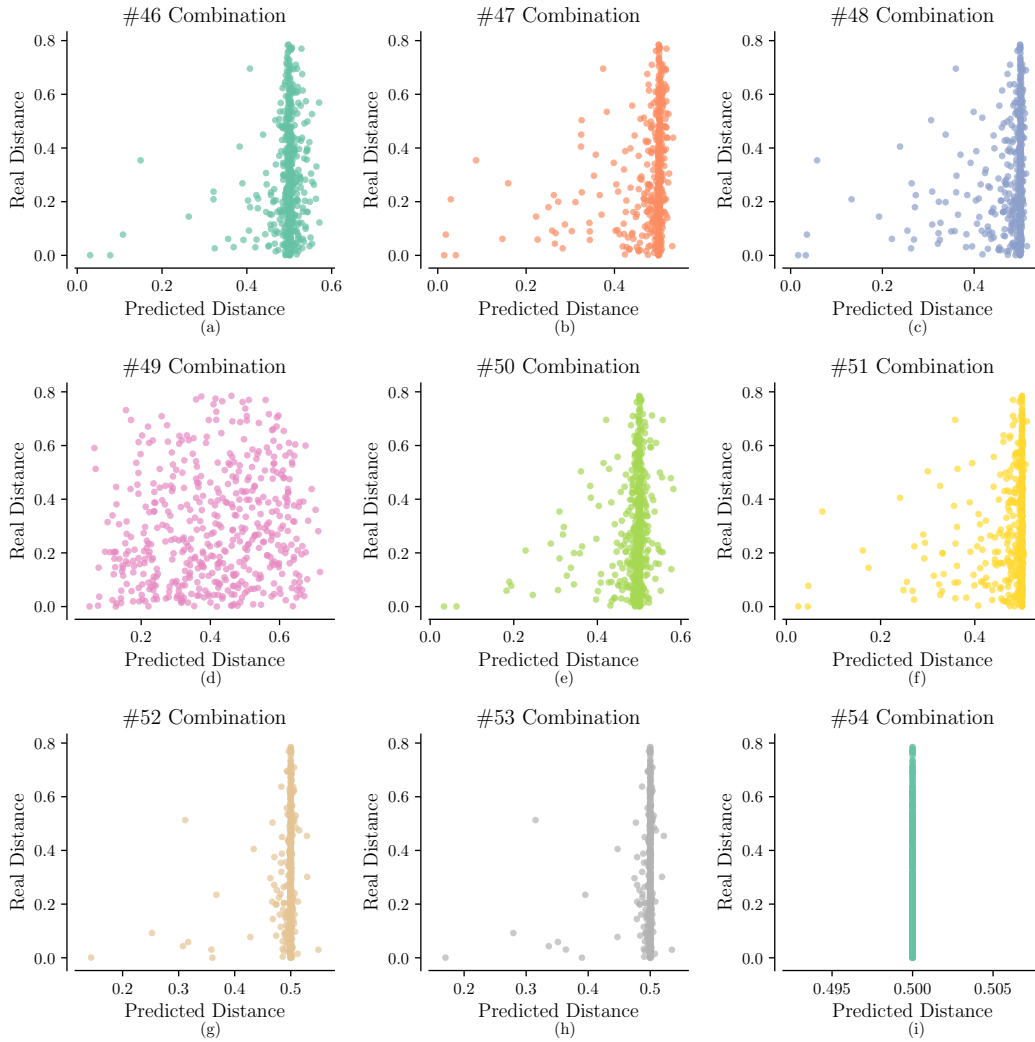


Figure 11: Qualitative performance of different kernel compositions (ranking #46 ~ #54).

Rank	Figure	Task Kernel	Configuration Kernel	Fidelity Kernel	ELBO
55	Figure 12 (a)	OptiLand	DeepLinear	Fabolas	0.1350
56	Figure 12 (b)	DeepLinear	Flat	Fabolas	0.1349
57	Figure 12 (c)	DeepLinear	Tree	Fabolas	0.1349
58	Figure 12 (d)	DeepLinear	DeepLinear	Fabolas	0.1349
59	Figure 12 (e)	DeepPoly	Flat	Fabolas	0.1349

Table 14: Quantitative performance of different kernel compositions (ranking #55 ~ #59).

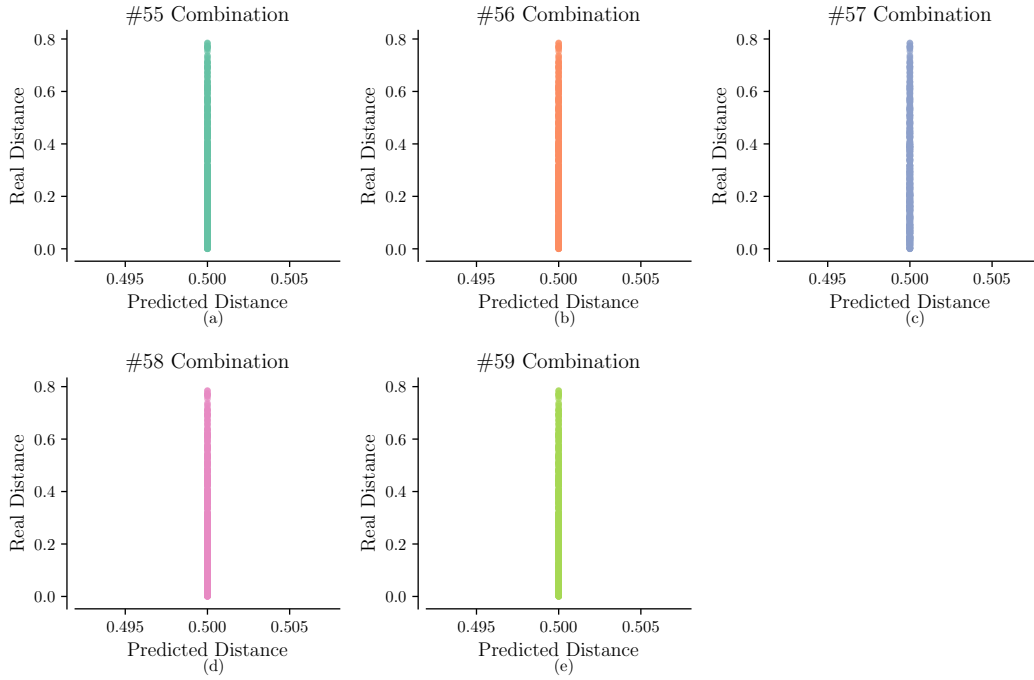


Figure 12: Qualitative performance of different kernel compositions (ranking #55 ~ #59).

Rank	Figure	Task Kernel	Configuration Kernel	Fidelity Kernel	ELBO
60	Figure 13 (a)	DeepPoly	Tree	Fabolas	0.1349
61	Figure 13 (b)	MTBO	DeepLinear	Fabolas	0.1342
62	Figure 13 (c)	MTBO	Flat	Fabolas	0.1342
63	Figure 13 (d)	MTBO	DeepPoly	Fabolas	0.1342
64	Figure 13 (e)	MTBO	Tree	Fabolas	0.1342

Table 15: Quantitative performance of different kernel compositions (ranking #60 ~ #64).

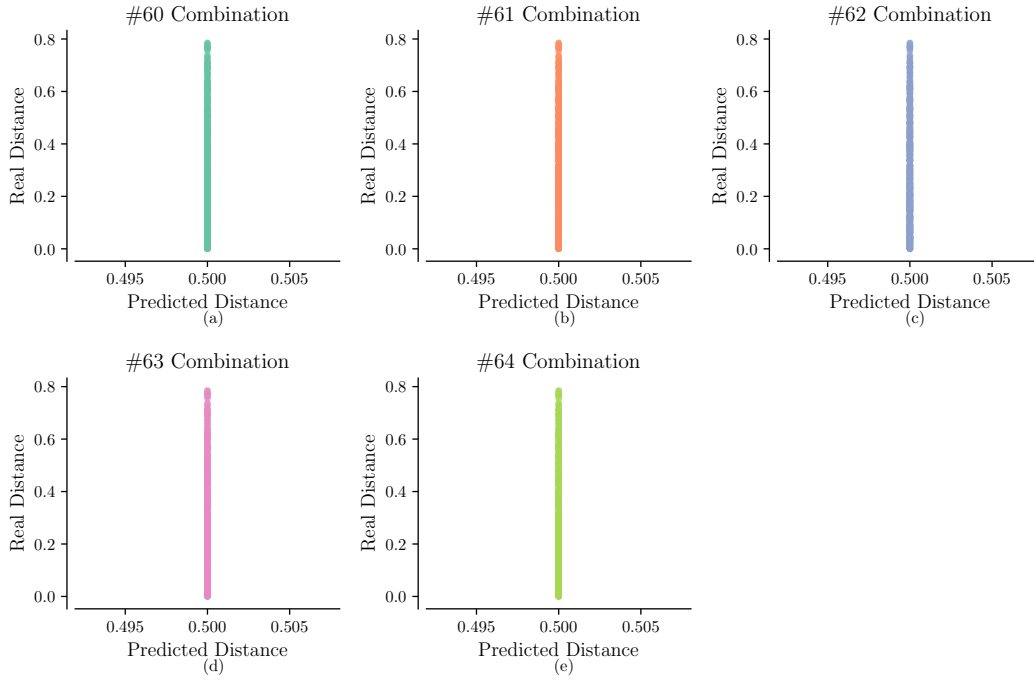


Figure 13: Qualitative performance of different kernel compositions (ranking #60 ~ #64).

D Experiment Details

We compare the proposed AT2 method against seven hyperparameter transfer learning baselines, based on our offline-computed database HyperRec and another real-world database LCBench [74]. Figure 14 shows AT2’s ability to transfer knowledge and forecast high-fidelity performance. Figure 15 shows the quantitative performance of AT2 and other baselines with one standard error. The detailed experiment setup is explained in Section 4.

We perform our experiments on an AWS P2 instance with one K80 GPU. It takes around one hour for AT2 to finish training and to run 100 queries on one train-test task pair. The GPyTorch package [14] uses the MIT license, and the LCBench database [74] uses the Apache License Version 2.0. The data used in our experiments contain the validation accuracy of machine learning models, and therefore do not include any personally identifiable information or require the consent of human subjects.

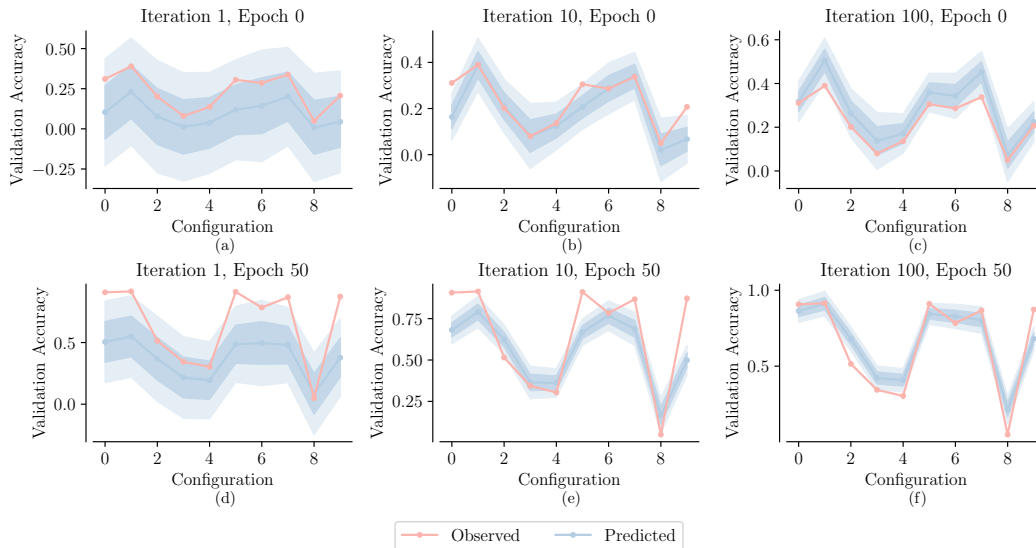


Figure 14: Predictions by AT2 versus observed validation accuracies for one sampled train-test task pair and 10 sampled configurations in HyperRec. The shaded regions indicate one and two predictive standard deviations. At iteration 1, AT2 approximates the optimization landscape of the new tuning task by transferring knowledge from past tasks. As more queries are made on the new task over iterations, AT2 better resembles the observed validation accuracies at both low and high fidelities (i.e., Epoch 0 and 50, respectively).

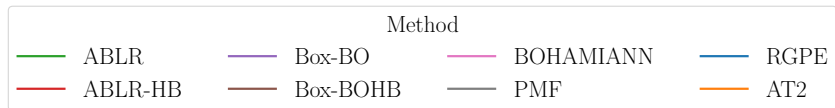
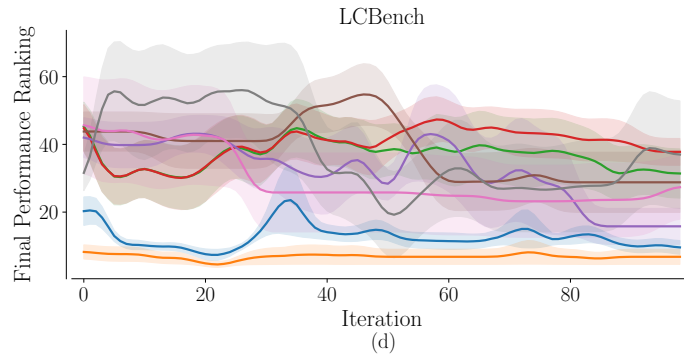
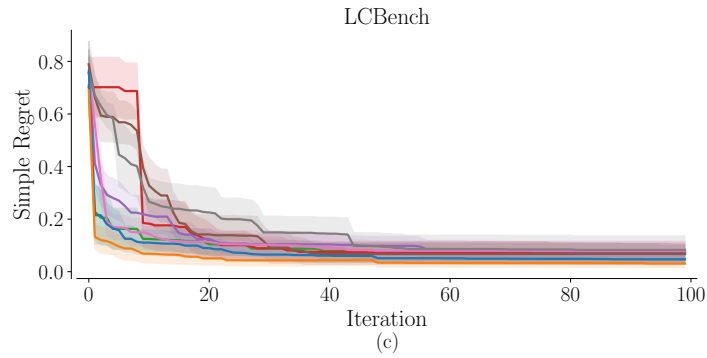
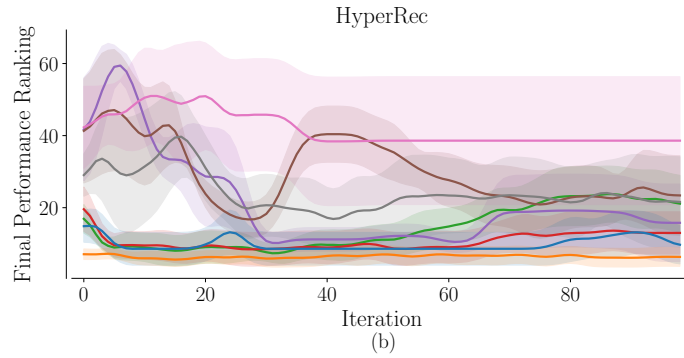
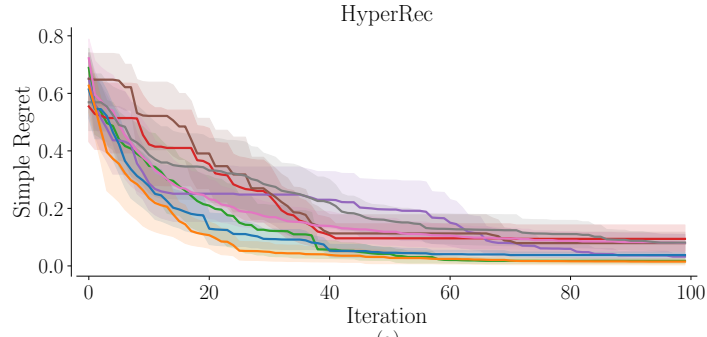


Figure 15: Performance of methods on HyperRec and LCBench. The results based on two metrics (simple regret and final performance ranking) are averaged across five train-test task pairs for each database. Lower is better. The predicted final performance rankings are smoothed with a hamming window of 10 iterations. The shaded regions represent one standard error of each method. Our proposed AT2 method consistently achieves lower simple regrets and final performance rankings.